EXPERIMENTAL INVESTIGATION OF ENERGY DISSIPATION THROUGH SCREENS

A THESIS SUBMITTED TO

THE GRADUATE SCHOOL OF NATURAL AND APPLIED SCIENCES

OF

THE MIDDLE EAST TECHNICAL UNIVERSITY

BY

PINAR ÇAKIR

IN PARTIAL FULFILLMENT OF THE REQUIREMENTS FOR THE DEGREE OF MASTER OF SCIENCE

IN

THE DEPARTMENT OF CIVIL ENGINEERING

AUGUST 2003

ABSTRACT

EXPERIMENTAL INVESTIGATION OF ENERGY DISSIPATION THROUGH SCREENS

Çakır, Pınar

M.Sc., Department of Civil Engineering

Supervisor: Assist. Prof. Dr. Zafer Bozkuş

Co-Supervisor: Prof. Dr. Metin Ger

August 2003, 70 pages

Screens may be utilized efficiently for dissipating the energy of water. In this study, water flowing beneath a gate is used to simulate the flow downstream of a hydraulic structure and screens are used as an alternative mean for energy dissipation. Investigations are done conducting a series of experiments. The porosity, thickness, and the location of the screens are the major parameters together with the Froude number of the upstream flow. The scope of this thesis covers the situation where there is a pseudo-jump formation. The experiments covered a range of Froude numbers between 5 and 18, porosities between 20% and 60%, and location of the screen up to 100 times of the undisturbed upstream flow depth. The thicknesses of the screens used are in the order of the undisturbed upstream flow depth. The results show the importance of each parameter on the energy dissipating performance of the screens and the system. It is observed that screens dissipate more energy than a jump within the range covered in these studies.

Keywords: Screen, energy dissipation, hydraulic jump, porosity, supercritical flow.

ÖZ

ELEKLERLE ENERJİ SÖNÜMLENMESİNİN
DENEYSEL ARAŞTIRILMASI

Çakır, Pınar
Yüksek Lisans, İnşaat Mühendisliği Bölümü
Tez Danışmanı: Yar. Doç. Dr. Zafer Bozkuş
Yardımcı Tez Danışmanı: Prof. Dr. Metin Ger

Ağustos 2003, 70 sayfa

Elekler, suyun enerjisinin kırılımı için uygun bir şekilde kullanılabilirler. Bu çalışmada bir hidrolik yapının mansabında gerçekleşen akışı göstermek için bir kapakla kontrol edilen su akımı kullanılmış ve enerjinin kırılımı için alternatif bir araç olarak elek kullanılmıştır. Araştırmalar bir dizi deney yapılarak uygulanmıştır. Ana parametreler geçirgenlik, elek kalınlığı, elek yeri ile birlikte memba akışının Froude sayısıdır. Bu tezin kapsamında sözde-sıçrama oluşumu durumu yer almaktadır. Araştırmalar kapsamında Froude sayıları 5 ve 18, boşluk oranları %20 ve %60 arasında değiştirilerek elek mesafesi için menba su derinliğinin 100 katına kadar ulaşan mesafeler kullanılmıştır. Kullanılan elek kalınlıkları menba su derinliği ile aynı mertebededir. Sonuçlar, her bir parametrenin eleklerin ve sistemin enerji kırılımı performansı üzerindeki önemini göstermektedir. Bu çalışmada kapsanan aralıkta eleklerin hidrolik sıçramadan daha fazla enerji kırdığı gözlenmiştir.

Anahtar Sözcükler: Elek, enerji kırılımı, hidrolik sıçrama, boşluk oranı, süperkritik akım.

To my parents...

ACKNOWLEDGMENTS

I would like to express my deepest gratitude and appreciation to Prof. Dr. Metin Ger for his precious guidance and support throughout my whole thesis study and my entire academic studies. In my future life I will try to reach his wide knowledge and appreciable humanity.

I would like to thank to Assist. Prof. Dr. Zafer Bozkus for his suggestions and support during my study.

I am deeply grateful to Yavuz Ozeren for his friendship and invaluable support, effort and patience throughout the whole thesis.

I wish to express my sincere appreciation to M. Kemal Cambazoglu for his precious support and friendship during every stage of my study.

I owe special thanks to all of my colleguages in Hydraulics Laboratory for being with me every time I need.

My special appreciation goes to Bahadir Dogan for his invaluable support and endless faith in me.

Finally, I would like to express my deepest gratitude to my family for their love, understanding, never ending support and unshakeable faith in me throughout my life.

TABLE OF CONTENTS

LIST OF TABLES

TABLE

LIST OF FIGURES

FIGURE

LIST OF SYMBOLS

A_0	area of the section 0 of the orifice-meter
A_1	area of the section 1 of the orifice-meter
A_2	area of the section 2 of the orifice-meter
C_0	discharge coefficient of the orifice-meter
C_C	contraction coefficient of the orifice-meter
C_V	contraction coefficient of vena contracta
d	gate opening
D_0	orifice throat diameter
D_1	pipe diameter on which the orifice meter located
D_{hole}	diameters of the screen holes
E_G	energy at section G
Fr_A	Froude number at section A
Fr_C	Froude number at section C
Fr_G	Froude number at section G
g	gravitational acceleration
h_L	head loss through the orifice-meter
k	distance between the screens of the double screen
L	theoretical length of a full jump
p	porosity of the screen
p_1	pressure at section 1 of the orifice-meter
p_2	pressure at section 2 of the orifice-meter
Q	flow rate
Q_{ideal}	ideal discharge for the orifice-meter
Re	Reynold's number
S	energy dissipated due to screen

t	thickness of the screen
V_1	velocity at section 1 of the orifice-meter
V_2	velocity at section 2 of the orifice-meter
V_A	average velocity at section A
V_C	average velocity at section C
w	width of the channel
X	distance between the screen and the gate
x	the distance from the upstream end of the pseudo-jump to the screen
y_A	water depth at section A
y_C	water depth at section C
y_G	water depth at section G
ΔE_{AB}	energy loss between sections A and B
ΔE_{AC}	energy loss between sections A and C
ΔE_{GC}	energy loss between sections G and C
ΔE_{jA}	energy loss due to a full jump at section A
ΔE_{jG}	energy loss due to a full jump at section G
α	a non-dimensional parameter defined in 3.3
β	a non-dimensional parameter defined in 3.2
ϕ	diameter ratio of the sections 0 and 1 for the orifice-meter
γ	specific weight of water
η_{scr}	screen efficiency
η_{sys}	system efficiency
μ	dynamic viscosity of water
ρ	density of water

CHAPTER I

INTRODUCTION

Control of the velocity and consequently the energy of water is a fundamental problem in hydraulic engineering. As water moves through the environment, whether by natural means or by human intervention, it is subject to continuous energy transformations. Since these continuous transformation processes constitute a major basis for implementations and theoretical analysis, it is very important for hydraulic engineers to understand these processes.

In order to avoid several destructive effects of excess energy of water, it should be extracted out. Flow control structures are used widely in order to keep this excess energy under control; even benefit from it in some cases. These control structures should meet some functional requirements; enough capacity to deliver the design discharge safely and dissipating the necessary amount of energy to protect hydraulic structure and downstream channel from localized erosion and scour.

Screens which are commonly used for several purposes in hydraulic and aerodynamic applications, seem to be efficient means of dissipating excess energy. A screen may be thought of as any distributed resistance that creates a change in flow direction and a reduction in energy. Laboratory work done so far suggests that the screens or porous baffles might be useful for energy dissipation downstream of small hydraulic structures. In this work, a series of experiments were carried out to

investigate the energy dissipation performance of screens.

Dimensional analysis and the preliminary runs made revealed that the porosity, thickness of the screen, and the location of the screen are the major parameters together with the Froude number of the upstream flow.

The experiments covered a range of Froude numbers between 5 and 18, porosities between 20% and 60%, and location of the screen up to 100 times of the undisturbed upstream flow depth.

In Chapter II, the previous works related to the screens used as energy dissipating means are summarized. In Chapter III, the conceptual frame of the thesis is given. In Chapter IV the experimental setup and procedures followed during data gathering are explained in details. The results including discussions are presented in Chapter V. The conclusions drawn are given in Chapter VI.

CHAPTER II

LITERATURE REVIEW

The earlier investigations on the flow through screens were generally performed by developing theoretical models. These models were verified with the experimental work conducted using airflow. The water flow through screens especially in conjunction with their energy dissipation characteristics has not been widely studied so far. Within this chapter the studies related to the content of this thesis are briefly introduced.

Baines and Peterson (1951) made an investigation on flow through screens and covered the effects of relatively coarse lattices and perforated plates placed perpendicular to a fluid flow. The effects investigated were divided into three main categories; the pressure drop across the screen, the modification of the velocity distribution caused by the screen, and the turbulence resulting from the screen. The investigations were conducted in air at high screen Reynolds numbers. However, the analysis was applicable to both liquids and gases.

The pressure drop was evaluated and the modification of the velocity distribution was investigated both theoretically and experimentally for various screen types and solidity ratios. The establishment and decay of turbulence downstream from screens were investigated experimentally. They concluded from these studies that there is a particular combination of screen characteristics which is most efficient

for a particular type of screen application. For example, a single screen made of large bars is more effective in the creation of turbulence, whereas several screens made of small bars are preferable in the dissipation of turbulence. For the elimination of variations in the velocity distribution, a series of uniform screens of low to moderate solidity ratio is indicated; on the other hand, for the production of the velocity variations, a single screen of correspondingly varied solidity ratio may be used. If a considerable dissipation of energy, i.e., reduction of pressure, is required, this may be obtained with a single screen of high solidity ratio-but at the expense of evenness in the velocity distribution. In all cases the shape of the screen elements is of secondary importance, in that it influences the energy loss but not the general distribution of velocity and turbulence.

During the experiments it was expected that for large Reynolds numbers the effect of *Re* on the pressure drop for any type of screen element would be insignificant. This expectation has been varied by these experiments.

Koo and James (1973) proposed a mathematical model for steady two-dimensional flow around a submerged screen. The general problem analyzed was the flow in a parallel-sided channel partially spanned by a screen, and the fluid was considered to be inviscid except at the screen, where the flow has the required pressure drop. The model was constructed by first replacing the screen with a distribution of sources and then manipulating the stream function for this flow so that the mass and momentum balances across the screen were satisfied. Consequently the model predicted a flow field, which was realistic except for the expected discontinuity in velocity between the wake and the external flow. The governing equations were solved numerically. The accuracy of the model was ascertained by wind-tunnel tests on screens. The theoretical results agreed well with the experimental data.

A survey conducted by *Laws and Livesey (1978)* divided the available literature on the topic of flow through screens into three categories (1) Investigations on characterizing the properties of the flow through a screen; (2) Investigations on

the effect of a screen on time-averaged velocity distributions; and (3) Investigations on the effect of a screen on turbulence distributions. The literature that they covered included *Koo and James's (1973)* study within category 2. However, the survey was mainly related to the Aeronautical applications

A prediction model was developed by *Yeh and Shrestha (1988)* for the headloss through a screen that is placed in an open channel. According to the study done, for a given approach-flow condition, screen inclination, and screen characteristics (i.e., flow contraction and deflection caused by a screen), values of the headloss could be predicted by the model. In the prediction model, it was assumed that the flow approaching the screen was uniform, and the frictional along the bottom boundary were negligible. When the flow passed through the screen, the flow was contracted by the limited opening area and deflected toward the direction normal to the screen surface. Since the contracted flow velocity at the leeward side of the screen was greater than the incident velocity, according to the Bernoulli theorem the pressure in front of the screen must be greater than that at its leeward side. This created a vertical pressure gradient owing to the screen inclination, and caused the flow deflection toward the direction normal to the screen. The flow behind the screen enhanced its turbulence, and the energy was dissipated due to this turbulent mixing process. The flow then became uniform in a region sufficiently far downstream from the screen.

The model proposed predicted that there is an optimal screen inclination to minimize the headloss. In order to verify the model, some experiments were performed with a wedgewire screen consisting of steel wires under the subcritical flow conditions. The results showed that there is an optimal inclination angle to minimize the headloss. The minimum of the headloss appeared to occur near 60^0 from the vertical. But the predicted value was 80^0. This discrepancy was due to the transverse support bars that appeared to create large flow disturbances, hence to dissipate the energy. The headloss for the vertical screen was somewhat higher than the predicted value. This could be explained by the formation of flow separation near the bottom boundary behind the screen. When the screen was inclined in the flow,

the flow separation was not present because of the flow deflection associated with the screen inclination.

Laboratory experiments conducted by *Rajaratnam and Hurtig (2000)* showed that screens or porous baffles with a porosity of about 40% could be used as effective energy dissipaters below small hydraulic structures, either in a single wall or a double wall mode. The experiments were carried out for a range of supercritical Froude numbers from about 4 to 13, and the relative energy dissipation was appreciably larger than that produced by the classical hydraulic jumps. Supercritical flow conditions were provided by a gate. First series of experiments were performed in a horizontal channel 0.45 m wide, 0.43 m deep and 6.3 m long. In the second series of experiments another 0.305 m wide, 0.7 m deep and 6 m long rectangular channel was used. A hard plastic screen with approximately square holes (of 5 mm sides) and an areal porosity of 40% was used to make single, double and triangular screens. The screen device was mounted perpendicularly across the flume at a distance of 1.25 m from the gate. These screens or porous baffles produced free hydraulic jumps, forced hydraulic jumps, and in some cases submerged jumps. The flow leaving these screens was found to be supercritical with a reduced Froude number.

Rajaratnam and Hurtig's (2000) study was considered as a stepping stone for this study for the investigation of energy dissipating characteristics of the screens. The experiments conducted within the scope of this thesis extended the available knowledge about screens as alternative energy dissipaters.

CHAPTER III

CONCEPTUAL FRAME

The flow just downstream hydraulic structures has been extensively studied. In order to dissipate the excess energy just downstream of a hydraulic structure, it is customary to impose a downstream control such that a jump is enforced to dissipate energy. In this study, flow beneath a gate is used to simulate the flow downstream of a hydraulic structure and screens are used as alternative means for energy dissipation.

3.1. Theoretical Base

To be able to scrutinize the effect of screens on the behavior of flow downstream of a gate, several preliminary experiments were performed. It is observed that a supercritical flow may show two distinct behaviors when it encounters a screen.

CASE 1:

The screen may lead to a jump such that the jump takes place far upstream of the screen. In other words, the screen is in the fully subcritical region. That is to say, the effectiveness of the screen as a mean of energy dissipater is minimal. Since the aim of this study is to investigate the effectiveness of the screen this case is left out

of the scope.

CASE 2:

The flow may impinge to the screen. Depending upon the Froude number the impinging jet either passes through the screen with some splashes back or may enforce a jump like behavior such that the screen is located within the zone which may be considered the roller zone if it were a jump. In either case, there is significant amount of energy dissipation. In other words, for both type of behaviors, there is pseudo-jump formation. For the analysis of this pseudo-jump formation the following conceptual frame is constructed (figure 3.1)

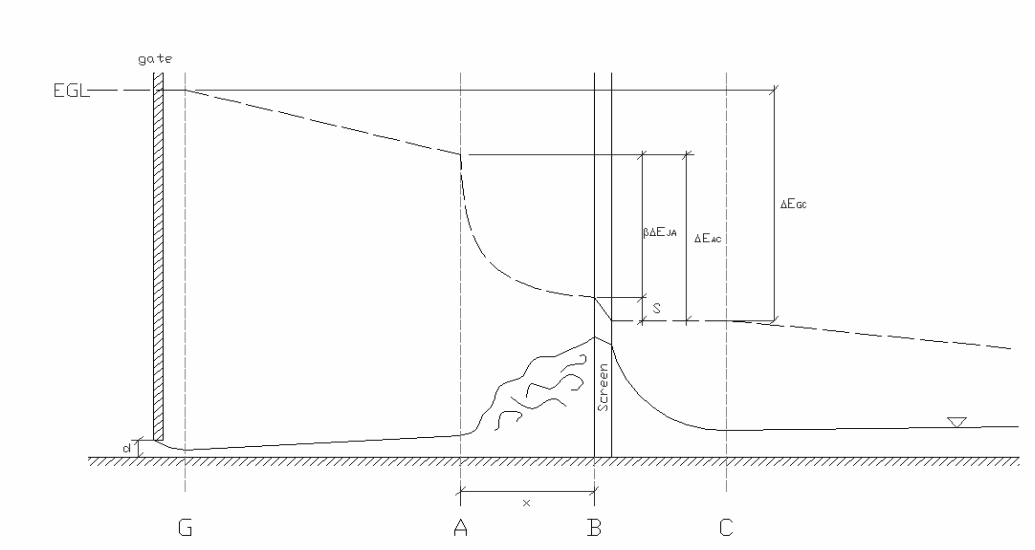

Figure 3.1 The general sketch for the flow pattern and energy loss definitions

The energy loss between section A and the screen is obtained using the expression

$$\Delta E_{AB} = \beta \Delta E_{jA} \tag{3.1}$$

where ΔE_{jA} is defined as energy loss due to a full jump that could be formed at section A.

The formula above is developed on the assumption that, the loss ΔE_{AB} is some function of the distance from the upstream end of the pseudo-jump, x, such that, β is defined as

$$\beta = e^{(1-\frac{1}{\alpha})} \tag{3.2}$$

where

$$\alpha = \frac{x}{L} \tag{3.3}$$

with L being the length of a jump if there were a full jump at section A. The reason an exponential form is adopted, is to take into account the extremities, full jump (Case 1) and impinging jet, and pseudo-jump formation (Case 2). For Case 1 the range of β is $\beta \geq 1$ and for Case 2 it is $0 < \beta < 1$ (see figures 3.2 and 3.3).

In equation 3.3, L is related to the Fr_A, after *French (1986)*, as

$$L = 9.75 y_A (Fr_A - 1)^{1.01} \tag{3.4}$$

with

$$Fr_A = \frac{V_A}{\sqrt{g y_A}} \tag{3.5}$$

where y_A , Fr_A ,V_A are the flow depth, Froude number and flow velocity respectively at section A and g is the gravitational acceleration.

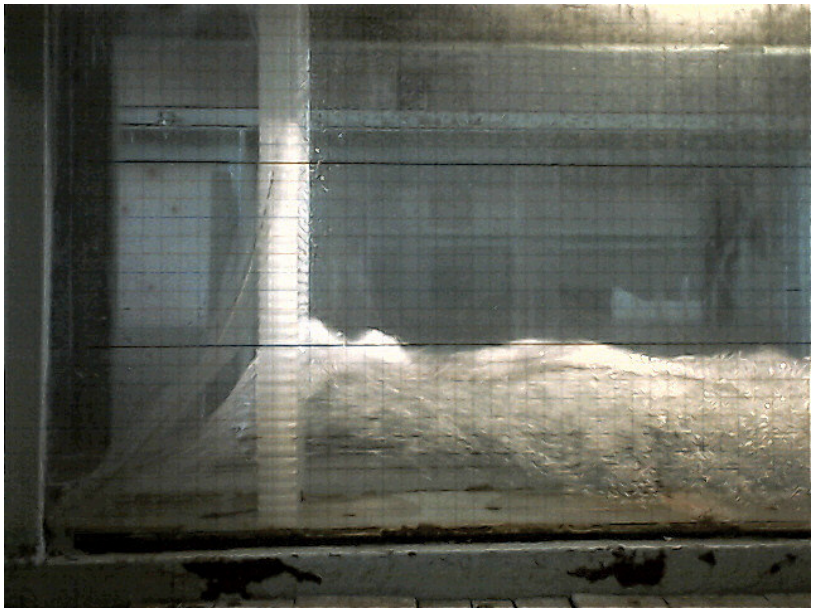

Figure 3.2 A sample view for Case 1

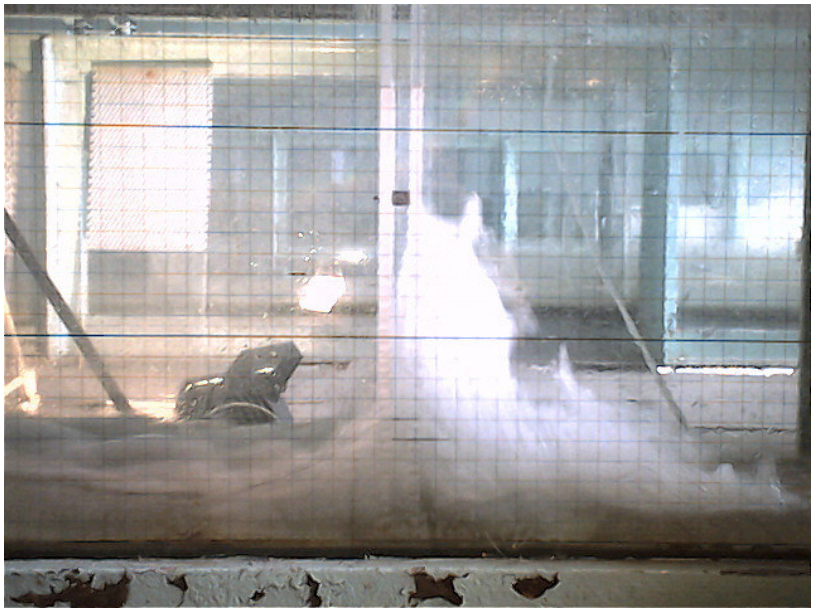

Figure 3.3 A sample view for Case 2

The energy loss through the screen, S, is

$$S = \Delta E_{AC} - \Delta E_{AB} \tag{3.6}$$

such that

$$S = (y_A + \frac{V_A^2}{2g}) - (y_C + \frac{V_C^2}{2g}) - \beta \Delta E_{jA} \tag{3.7}$$

where y_C and V_C is the flow depth and flow velocity respectively at section C.

To assess the performance of the screen either the total energy lost between the gate and the section just downstream of the screen, ΔE_{GC} or the energy lost through the screen, S, can be used. The system loss, ΔE_{GC} is defined as

$$\Delta E_{GC} = (y_G + \frac{V_G^2}{2g}) - (y_C + \frac{V_C^2}{2g}) \tag{3.8}$$

where y_G is the depth at the vena contracta defined as

$$y_G = C_V \cdot d \tag{3.9}$$

and $C_V = 0.625$ after *Simon (1981)*

Based on these performance criteria, the efficiency of the system η_{sys} and the efficiency of the screen η_{scr} are defined such that

$$\eta_{sys} = \frac{\Delta E_{GC} - \Delta E_{jG}}{\Delta E_{jG}} \tag{3.10}$$

and

$$\eta_{scr} = \frac{S}{\Delta E_{jG}} \tag{3.11}$$

3.2. Dimensional Analysis

Based on the theoretical investigation of the flow between the gate and the screen, the following parameters were identified to form a basis for the dimensional analysis such that

$$S = f_1(Q, d, w, y_G, y_A, y_C, x, X, p, k, t, g, \rho, \mu) \tag{3.12}$$

where

S: energy dissipated due to screen, [L],

Q: discharge, [L^3T^{-1}],

d: gate opening, [L],

w: width of the channel, [L],

y_G: water depth at section G, [L],

y_A: water depth at section A, [L],

y_C: water depth at section C, [L],

x: the distance from the upstream end of the pseudo-jump to the screen, [L],

X: distance between the screen and the gate, [L],

p: porosity of the screen,

k: distance between the screens of the double screens, [L],

t: thickness of the screen, [L],

g: gravitational acceleration, [LT^{-2}],

ρ: density of water, [ML^{-3}],

μ: dynamic viscosity of water, [$ML^{-1}T^{-1}$)]

Recalling the fact that E_G, energy at section G, [L], L being the length of jump if there were a full jump at section A, [L], and Fr_C, Froude number just downstream the screen, are functions of

$$E_G = f_2(g, y_G, d, w, Q) \tag{3.13}$$

$$L = f_3(g, w, Q, y_A) \tag{3.14}$$

$$Fr_C = f_4(g, w, Q, y_C) \tag{3.15}$$

Thus replacing w, y_A, y_C in equation 3.12 by E_G, L and Fr_C respectively, one obtaines

$$S = f_5(E_G, y_G, d, Q, L, Fr_C, x, X, p, k, t, g, \rho, \mu) \tag{3.16}$$

Selecting y_G, g and ρ as repeating variables the following non-dimensional form of equation is obtained as

$$\frac{S}{y_G} = f_6(\frac{E_G}{y_G}, Fr_G, \frac{L}{y_G}, Fr_C, \frac{x}{y_G}, \frac{X}{y_G}, p, \frac{k}{y_G}, \frac{t}{y_G}, \frac{y_G}{d}, Re) \tag{3.17}$$

where Re is the Reynolds number.

The above equation can be put into more convenient form as follows:

$$\frac{S}{E_G} = f_7(Fr_G, \alpha, \frac{X}{d}, p, \frac{k}{t}, \frac{t}{d}, \left| Fr_C, \frac{E_G}{d}, \frac{x}{d}, C_V, Re \right|) \tag{3.18}$$

where α is as defined in equation 3.3.

The three of the last five parameters namely Fr_C, $\frac{E_G}{d}$, and $\frac{x}{d}$ are irrelevant to the scope of this study. C_V which is defined as $\frac{y_G}{d}$ is a constant. As to the *Re*, the magnitude of Fr_G is relatively high in the range covered during the experiments therefore there is no dependence of the flow behavior on the Reynolds number. Hence, dropping those terms the final form of the non-dimensional relationship among the parameters is obtained as given below.

$$\frac{S}{E_G} = f_8(Fr_G, \alpha, \frac{X}{d}, p, \frac{k}{t}, \frac{t}{d}) \tag{3.19}$$

The experimental setup is designed and constructed considering the parameters in equation 3.19, which form the basis for the energy dissipating characteristics of the screens from the hydraulics engineering perspective. The details of the setup and the experimental procedure are included in Chapter IV.

CHAPTER IV

THE EXPERIMENTAL INVESTIGATIONS

Within the conceptual frame work introduced above, experiments are performed to measure the performance of screens as energy dissipaters. The properties of the experimental setup and the details of the experimental procedure are explained in the following sections.

4.1 Experimental Setup

Experiments are conducted on a horizontal open channel model 7.5 m long having a rectangular cross section. The channel cross section is 29 cm wide and 70 cm deep. The channel bottom is covered with Plexiglas to provide a smooth surface that is of compatible roughness with that of glass. A constant head tank provides the required discharge values and a pipe with a valve on it carries the water to the metal box having an opening at its bottom. An orifice-meter is placed on the pipe to measure the flow rate. Measurement of the depths is performed by a mobile point gage attached to the channel. A number of screens with different porosities are prepared for the experiments. A detailed schematic view of the channel and the whole setup is given in figures 4.1, 4.2 and 4.3.

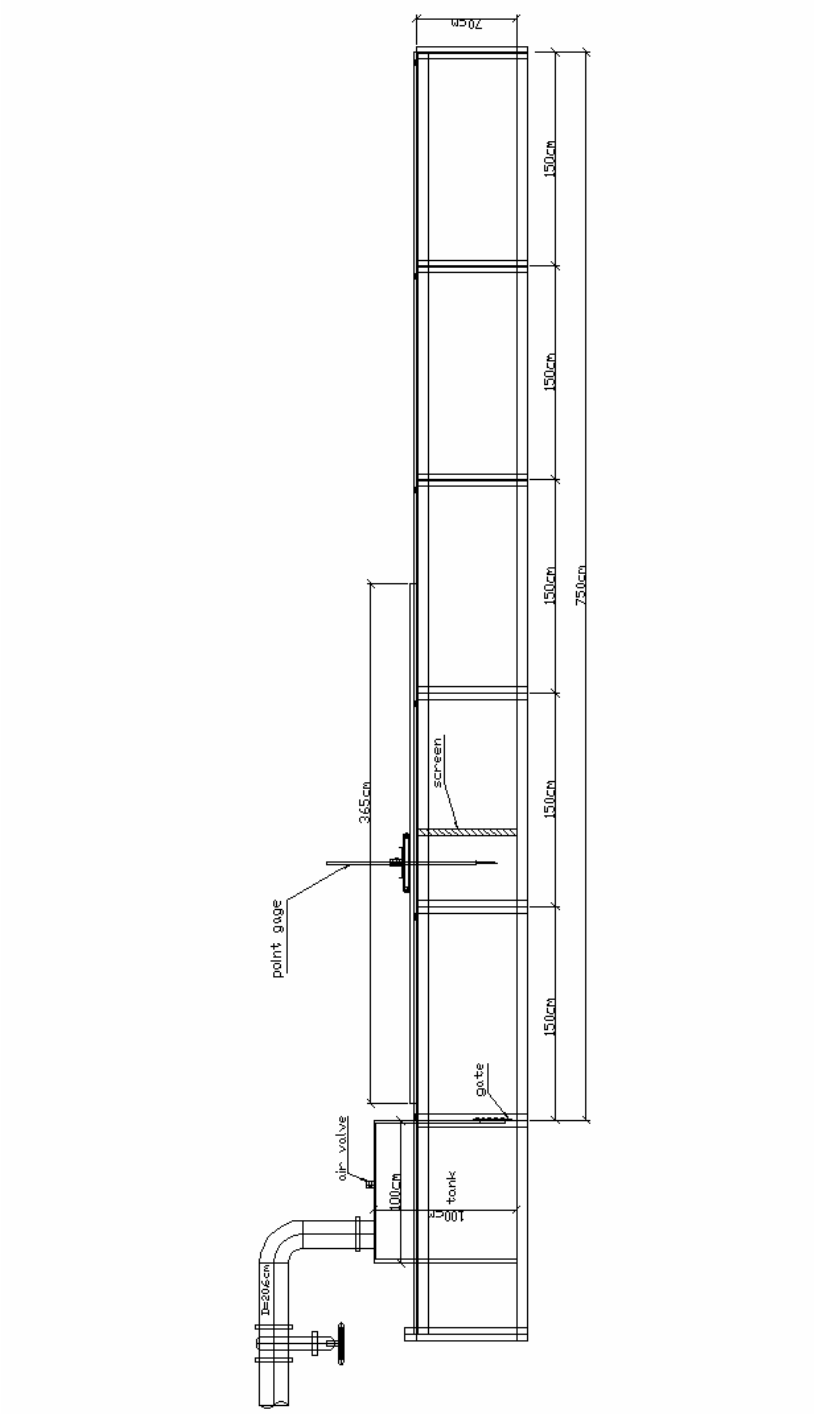

Figure 4.1 Side view of experimental setup

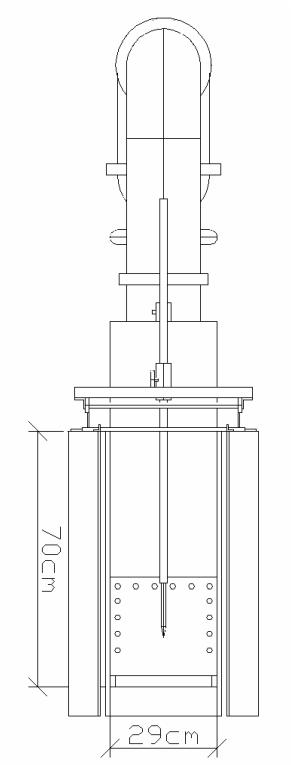

Figure 4.2 Front view of the setup

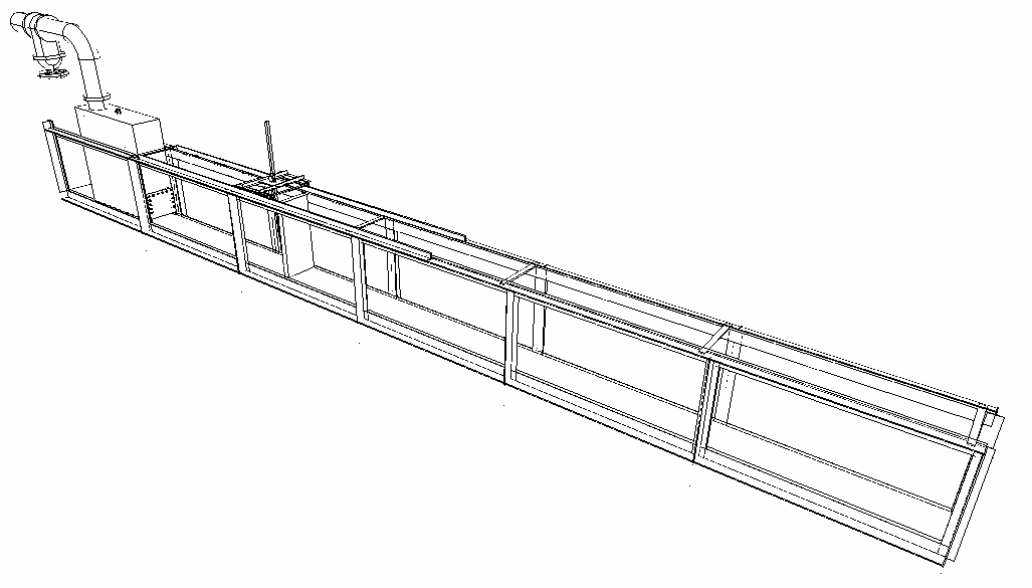

Figure 4.3 A general view of the setup

4.1.1 Gates

The rectangular opening at the bottom of the metal box acts like a sluice gate and it is obtained by placing a gate of iron sheet screwed to the box that can be replaced during experiments. This gate maintains the upstream supercritical flow conditions required for the experiments. Froude number range covered during the experiments is from 5 to 18 and this wide spectrum is provided effectively with three different gate openings of 2cm, 3cm and 4cm. Assuming that there is no head loss between the exit of the gate and the vena contracta, all the initial energy calculations are done with respect to the depth at vena contracta.

4.1.2 Screens

The major components of the set up are the screens made up of Plexiglas of 1cm thickness. This material is chosen for the experimental work since it is handled easily while giving required porosity values. Different porosities, 20%, 40%, 50% and 60% are obtained by drilling 1cm diameter holes arranged with a uniform triangular mesh. The 2cm, 4cm and 4D (two screens arranged to form a 2cm gap between them) arrangements are constructed using single 1cm thick Plexiglas screens (figures 4.4, 4.5 and 4.6). In order to fix the screens rigidly wherever it is required, a simple mechanism is developed and installed onto the screens. The screens are placed perpendicularly into the channel so that they are orthogonal to the flow and anchored to the bottom at a distance providing consistent *X/d* values for different gate openings.

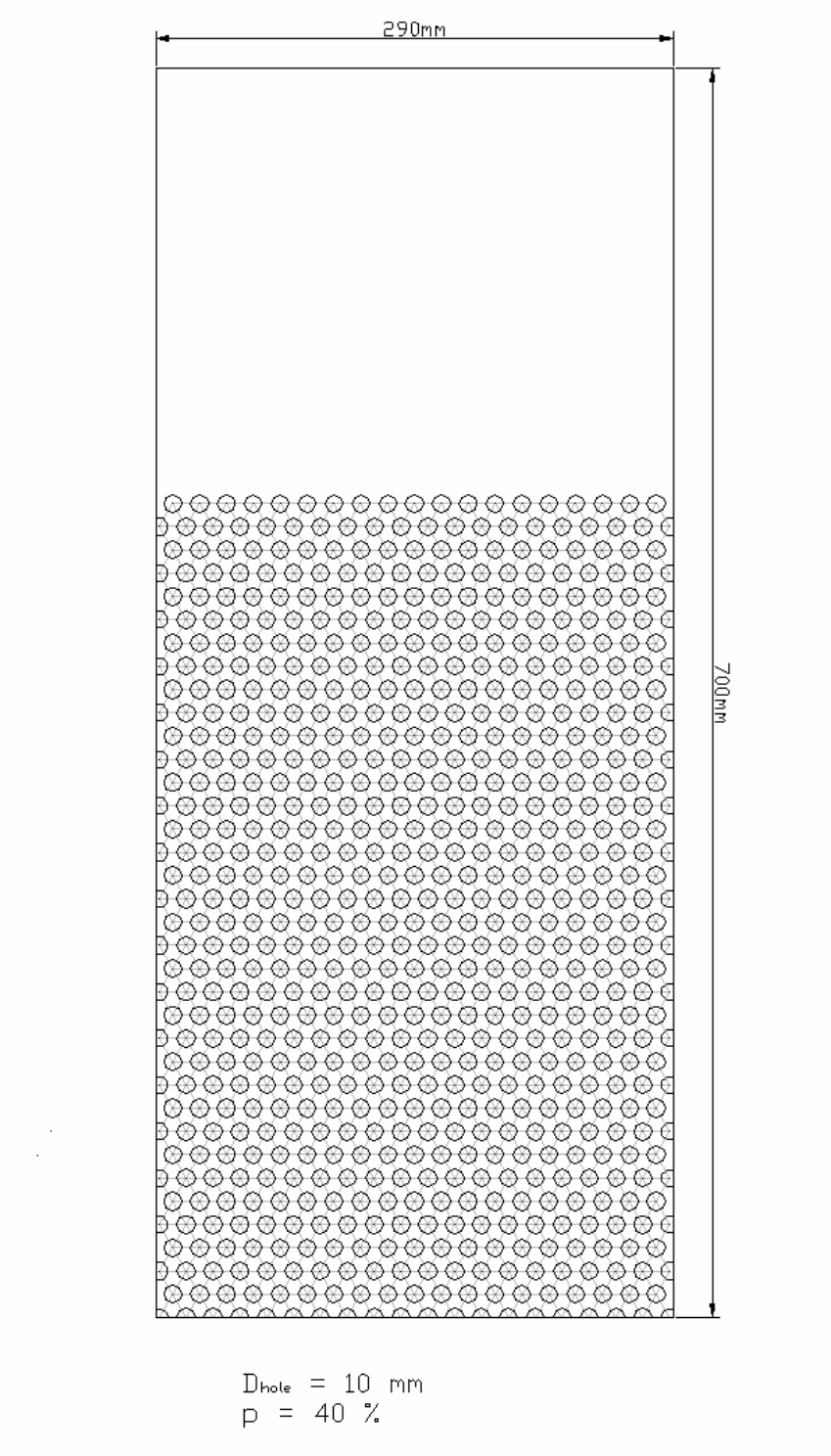

Figure 4.4 The screen of porosity 40%

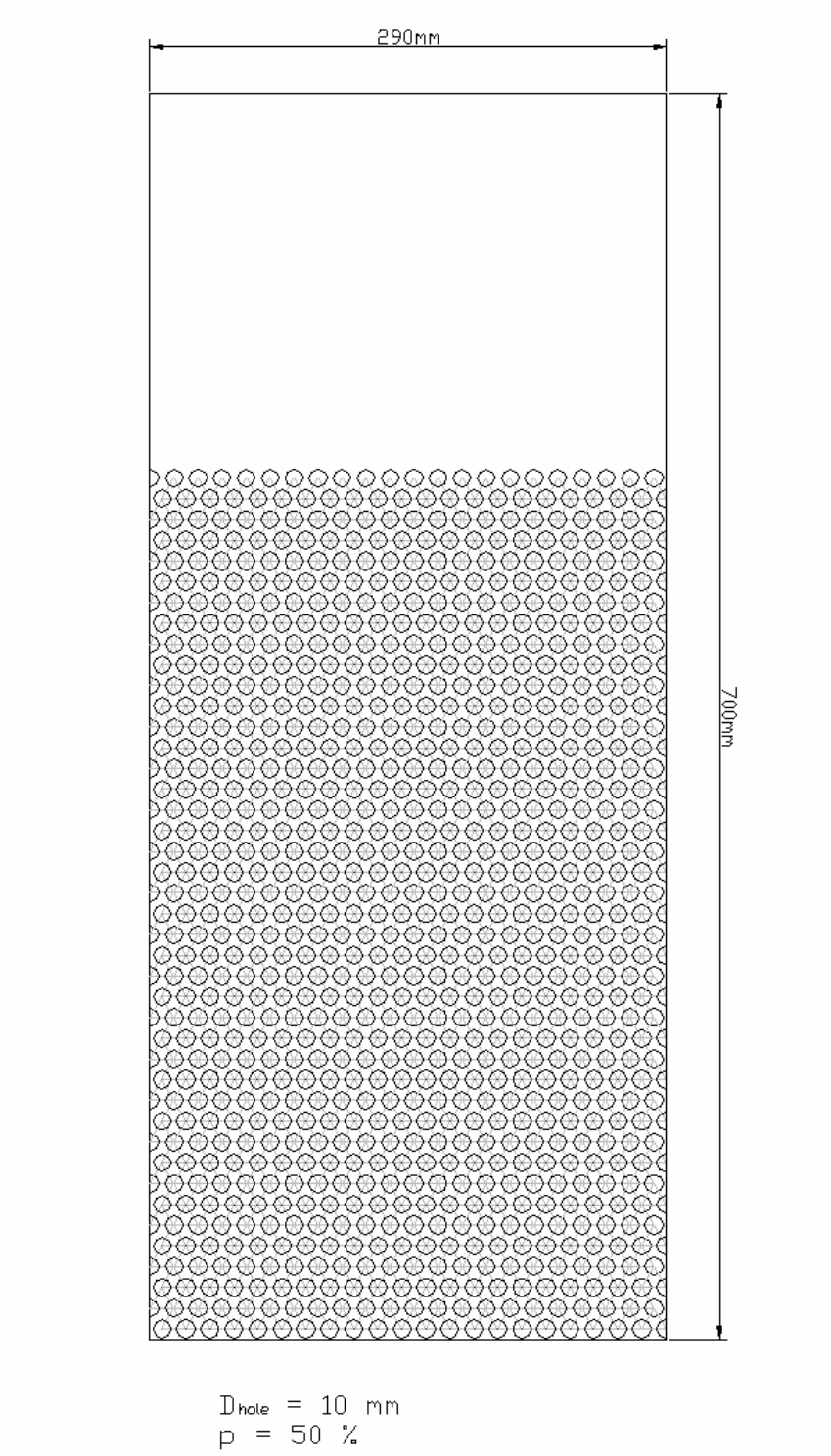

Figure 4.5 The screen of porosity 50%

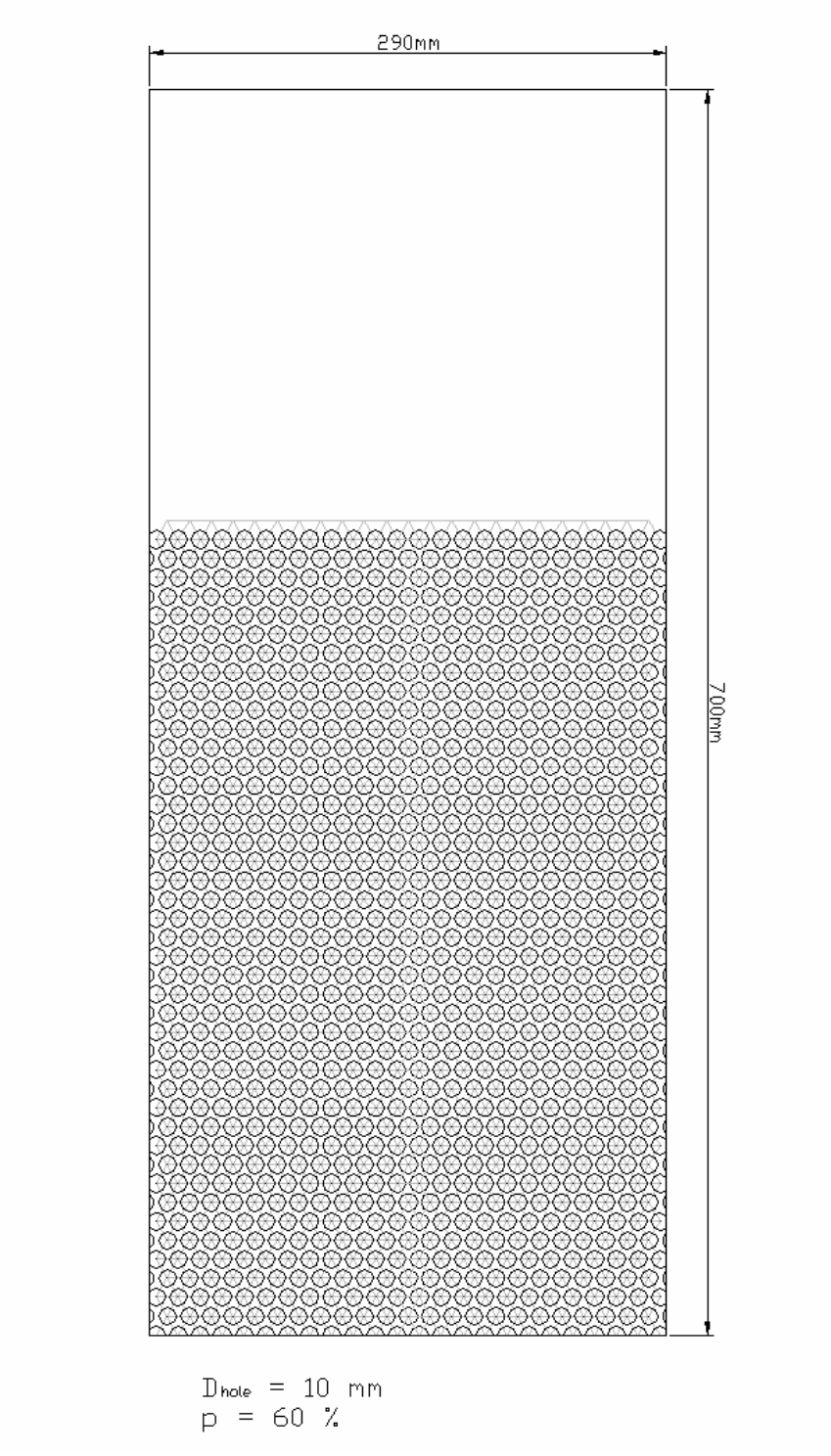

Figure 4.6 The screen of porosity 60%

4.1.3 Determination of Flow Rate by the Orifice-meter

An orifice meter is constructed whose design details are determined after investigating Institution of Turkish Standards (TSE) requirements. The orifice-meter is located on the pipe extending from the head tank and the required discharge levels are obtained by adjusting the valve on the pipe while observing the manometer readings connected to the orifice-meter.

The orifice meter used consists of a flat Plexiglas orifice plate with a circular hole drilled on it. There is a pressure tap upstream from the orifice plate and another just downstream. To measure pressure head on the orifice, a 30^0 inclined mercury manometer connected to the tabs is used in the experiments.

A detailed drawing of the orifice meter and implemented TSE requirements are given in the Appendix A.

4.2 Experimental Procedure

In reference to equation 3.19, the experiments are scheduled to investigate the performance of the screens for several combinations of the variables. In table 4.1, the combination of variables for which experiments were run, are marked with '✓ '. Those combinations of variables for which experiments were not run, marked with '*x*', are the situations under which either Case 2 (see page 8) condition did not prevail or the experimental setup is not suitable to take measurements.

Table 4.1 The list of experiments (symbol '✓' denotes the ones conducted, symbol *'x'* denotes the experiments not conducted)

X/d	***t/d***	***40%***	***50%***	***60%***	***t/d***	***40%***	***50%***	***60%***	***t/d***	***40%***	***50%***	***60%***
33	***1***	*x*	*x*	*x*	***0.33***	*x*	*x*	*x*	***0.5***	*x*	*x*	*x*
	2	*x*	*x*	*x*	***1.33***	✓	✓	✓	***1***	✓	✓	✓
	2D	*x*	*x*	*x*	***2D***	*x*	✓	✓	***1D***	*x*	✓	✓
66	***1***	*x*	*x*	*x*	***0.33***	✓	*x*	✓	***0.5***	*x*	*x*	*x*
	2	✓	✓	✓	***1.33***	✓	✓	✓	***1***	✓	✓	✓
	2D	✓	✓	✓	***2D***	✓	✓	✓	***1D***	✓	✓	✓
99	***1***	*x*	*x*	*x*	***0.33***	✓	*x*	✓	***0.5***	*x*	*x*	*x*
	2	✓	✓	✓	***1.33***	✓	✓	✓	***1***	*x*	*x*	*x*
	2D	✓	✓	✓	***2D***	✓	✓	✓	***1D***	*x*	*x*	*x*

The preliminary runs with p=20% have proven that within the physical capabilities of the setup, Case 2 conditions are never realized. Hence, these runs were not included in table 4.1.

For each set of experiment, after fixing a gate opening (d) 2cm, 3cm or 4cm, the screen is placed into the channel at distances providing consistent *X/d* values. The nominal X values are determined as given in table 4.2.

Table 4.2 The nominal X values and the gate openings

X(cm)	***d=2cm***	***d=3cm***	***d=4cm***
X/d=33	***66***	***100***	***133***
X/d=66	***133***	***200***	***267***
X/d=99	***200***	***300***	***400***

Once the screen is placed properly into the channel, discharge values are set using the valve on the pipe connected to the tank. In each set, the maximum and the minimum discharge values are determined observing the behavior of water. The discharge is raised as much as possible providing that it is still possible to take water surface readings accurately. And the discharge is lowered until the water starts to choke the gate and it becomes impossible to measure the depth. Several discharge values are adjusted by the valve between these limiting ends. In order to calculate the flow rate, the orifice meter with a mercury manometer connected to it is utilized. Following the adjustment of the valve, the readings are taken from the manometer and recorded. Then, on sections A and C, the depth of flow is measured with point

gage at four points covering the axes of the sections in order to be more accurate. The average of these four values is used during the calculations. The locations of the sections A, the upstream section of the jump or pseudo-jump, and C, vena contracta downstream the screen, are determined based on the observations.

With the completion of one set of experiment, the location of the screen is changed. For a given gate opening, different screens of 2 cm, 4cm and 4D, with porosities of 40%, 50% and 60% are fixed on the predetermined locations. This procedure is repeated for each gate opening.

CHAPTER V

RESULTS AND DISCUSSIONS

5.1. Introduction

The findings of the experimental study are presented below in a systematic way in the form of graphics. The original data are given in Appendix B.

The naming convention which makes reference to the independent variables appearing in equation 3.19 is developed such that both the graphical summaries and the original data can be properly identified. The naming convention is explained by two examples given below.

Table 5.1 The reference key

Reference	*Porosity*	*t/d*	*X/d*	Fr_G
40-2D-99-13.98	*40%*	*2(double)*	*99*	*13.98*
50-1-33-9.35	*50%*	*1*	*33*	*9.35*

Yet, for the graphical representation of the data since variations are plotted against Fr_G, Froude number values were dropped out of the labels.

5.2. Performance of the system

As indicated before the total energy loss between the exit of the gate and the downstream of the screen is denoted as ΔE_{GC}. This energy loss includes the friction losses, losses due to the pseudo-jump and the screen loss. The relative energy loss $\Delta E_{GC}/E_G$ is used to analyze the system performance.

5.2.1. Performance of the system at large

The figures 5.1, 5.2, 5.3, 5.4, 5.5 and 5.6 showing the variation of $\Delta E_{GC}/E_G$ with Froude number at the vena contracta downstream the gate, Fr_G, are given both for single and double screens. Variations are shown for each *X/d* separately.

On the same graphs, the energy loss that would have been realized if there were a jump at section G is also depicted by a solid line for comparison purposes.

From the graphics, one may discern that

i. $\Delta E_{GC}/E_G$ increases with Fr_G.

ii. $\Delta E_{GC}/E_G$ becomes more dependent on the porosity with increasing Fr_G. Yet the dependence is weaker for double screens.

iii. Dependence of $\Delta E_{GC}/E_G$ on the porosity with increasing Froude number becomes less apparent with increasing *X/d*.

iv. No apparent dependence on *t/d*. This may be due to the fact that the range of *t/d* covered is ‘thin’.

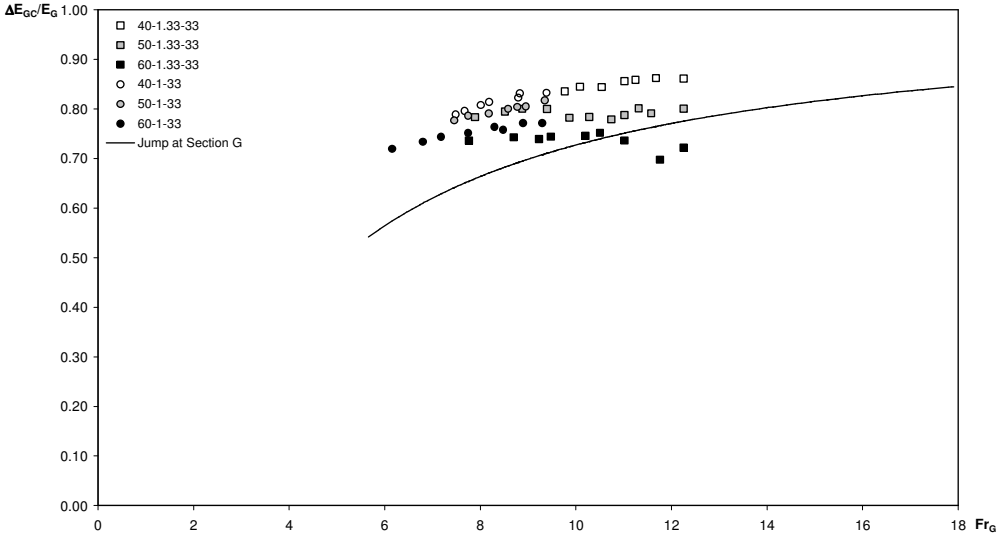

Figure 5.1 $\Delta E_{GC}/E_G$ vs. Fr_G for single screens at X/d=33

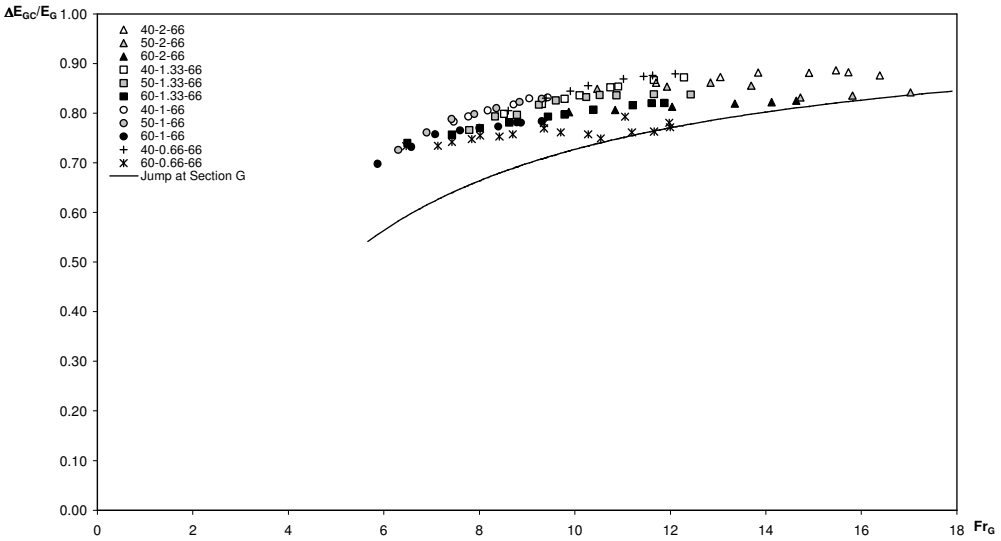

Figure 5.2 $\Delta E_{GC}/E_G$ vs. Fr_G for single screens at X/d=66

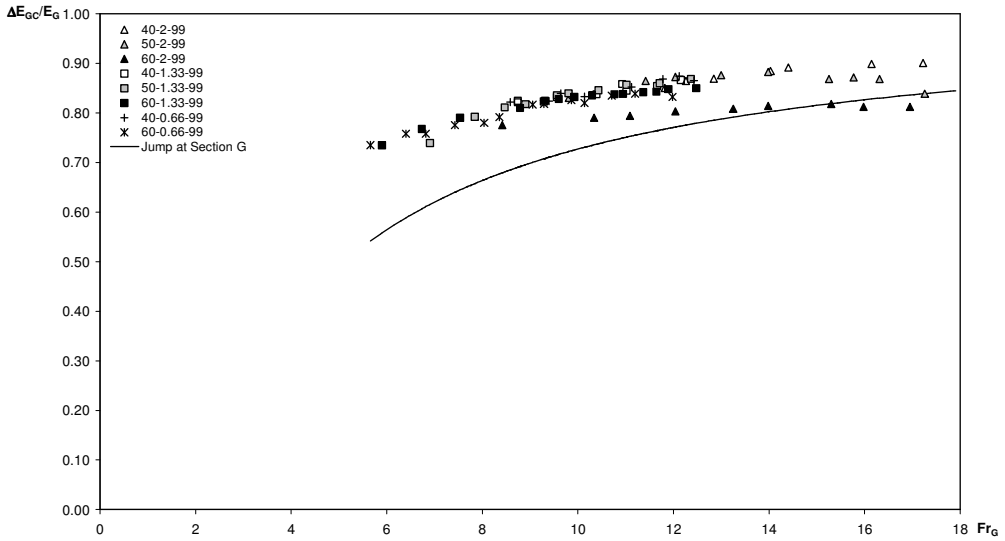

Figure 5.3 $\Delta E_{GC}/E_G$ vs. Fr_G for single screens at X/d=99

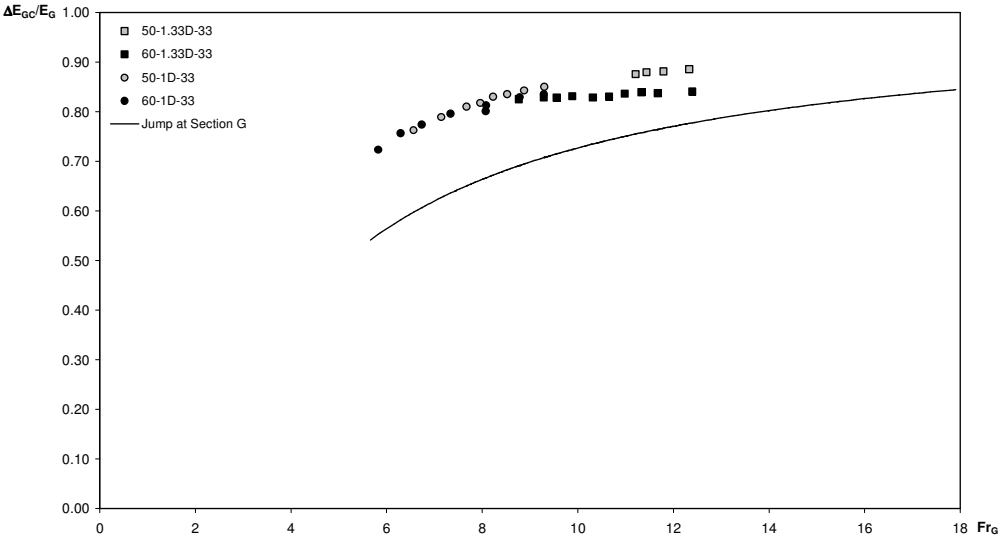

Figure 5.4 $\Delta E_{GC}/E_G$ vs. Fr_G for double screens at X/d=33

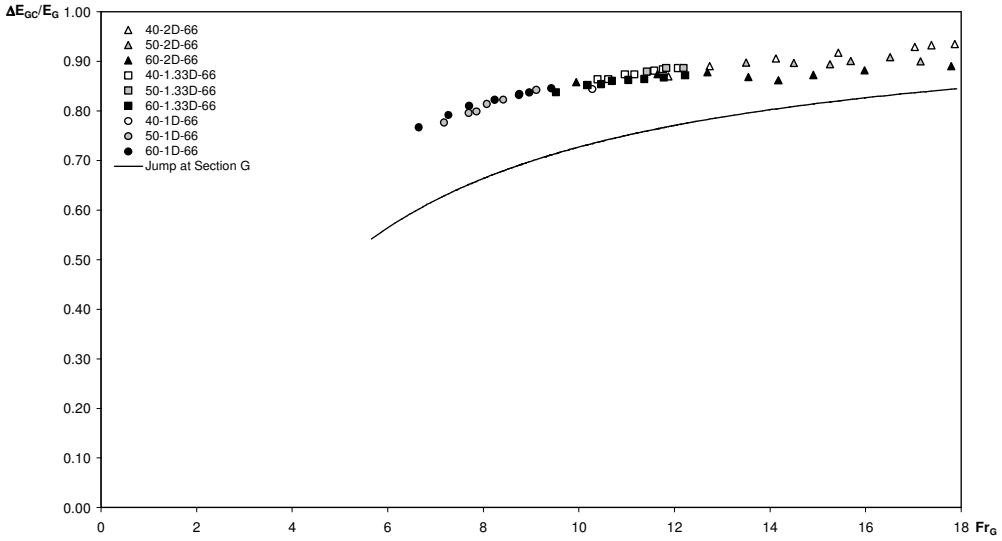

Figure 5.5 $\Delta E_{GC}/E_G$ vs. Fr_G for double screens at X/d=66

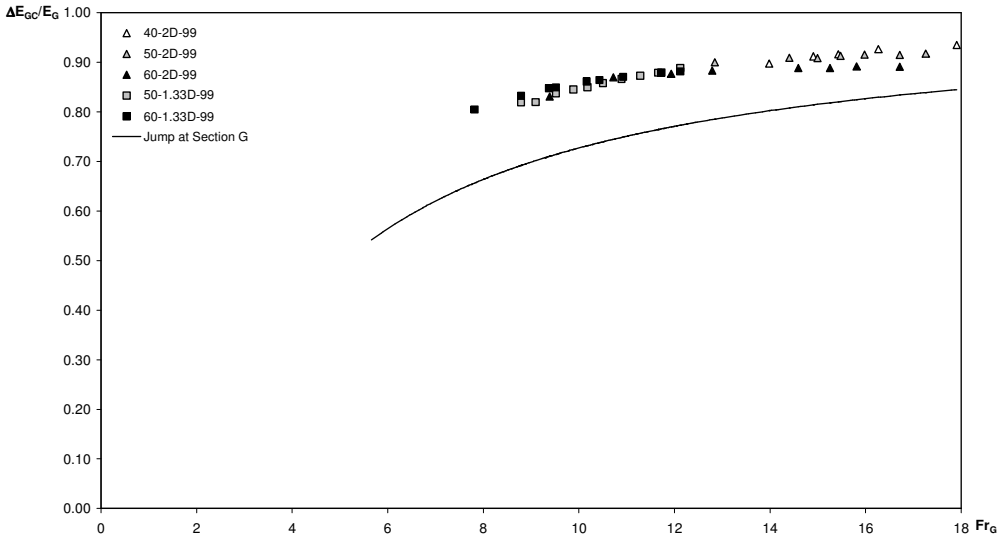

Figure 5.6 $\Delta E_{GC}/E_G$ vs. Fr_G for double screens at X/d=99

5.2.2. Comparison of present data with that of Rajaratnam and Hurtig

Rajaratnam and Hurtig conducted experiments using double screens with a 40% porosity mounted at a distance 1.25 m from the gate. A hard plastic screen with approximately square holes (of 5 mm sides) was used to make these double screens. In the first set, the space between the screens was equal to 26 mm and in the second set it was 54 mm. The gate opening was 25.4 mm. As shown in figure 5.7 in which Rajaratnam and Hurtig's data is compared with that part of present data with compatible characteristics, there is an agreement between the data.

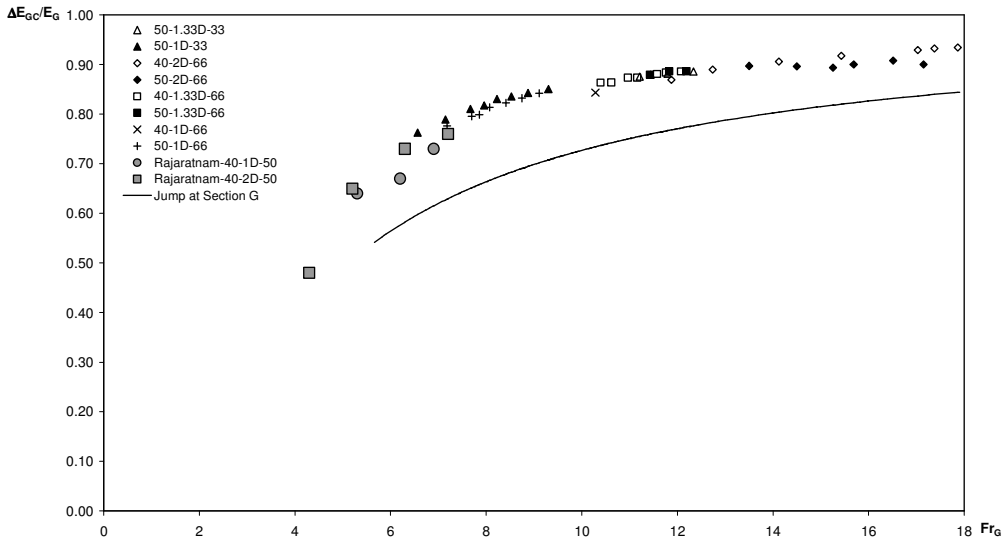

Figure 5.7 Comparison of Rajaratnam and Hurtig's data with that of present work compatible with it

5.2.3. Comparison of system performances of single and double screens

The effect of so called double screens on the system performance is demonstrated in figures 5.8, 5.9, 5.10, 5.11, 5.12, 5.13, 5.14 and 5.15. After the examination of these figures one may discern that

i. Double screens are more efficient for the range covered.

ii. Efficiency of the double screens becomes more pronounced with increasing Fr_G.

iii. Yet, with increasing *X/d*, the effectiveness of the double screens becomes less pronounced.

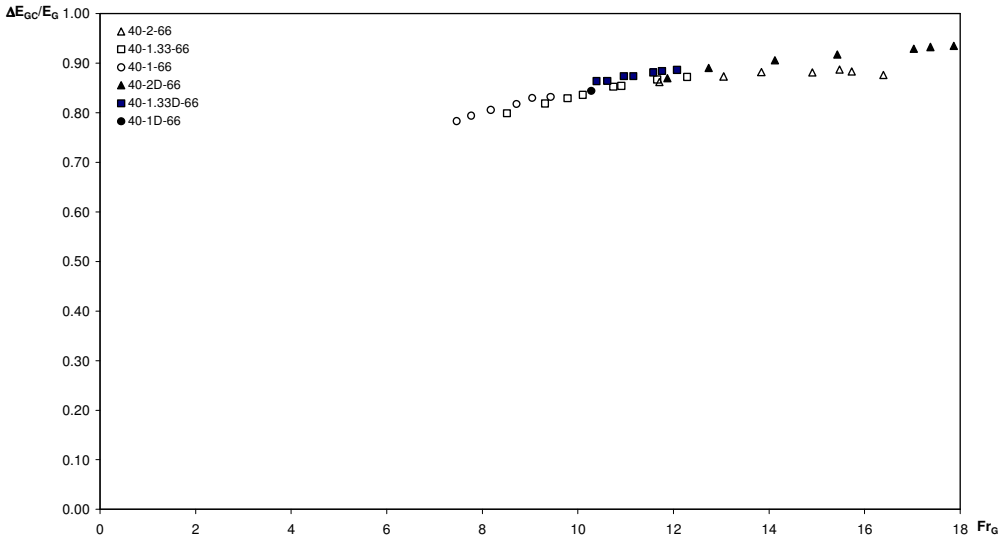

Figure 5.8 $\Delta E_{GC}/E_G$ vs. Fr_G for p=40% at X/d=66 for the comparison of single and double screens

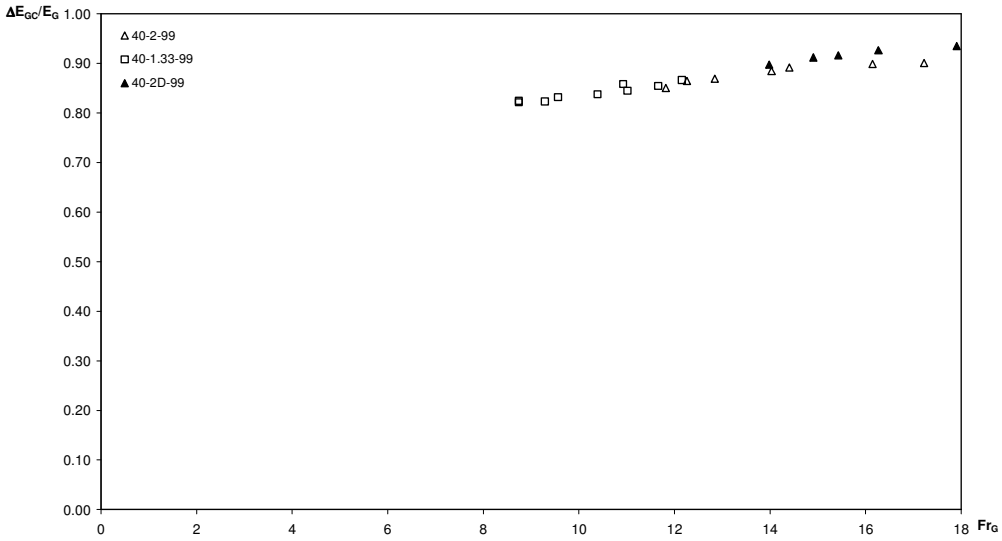

Figure 5.9 $\Delta E_{GC}/E_G$ vs. Fr_G for p=40% at X/d=99 for the comparison of single and double screens

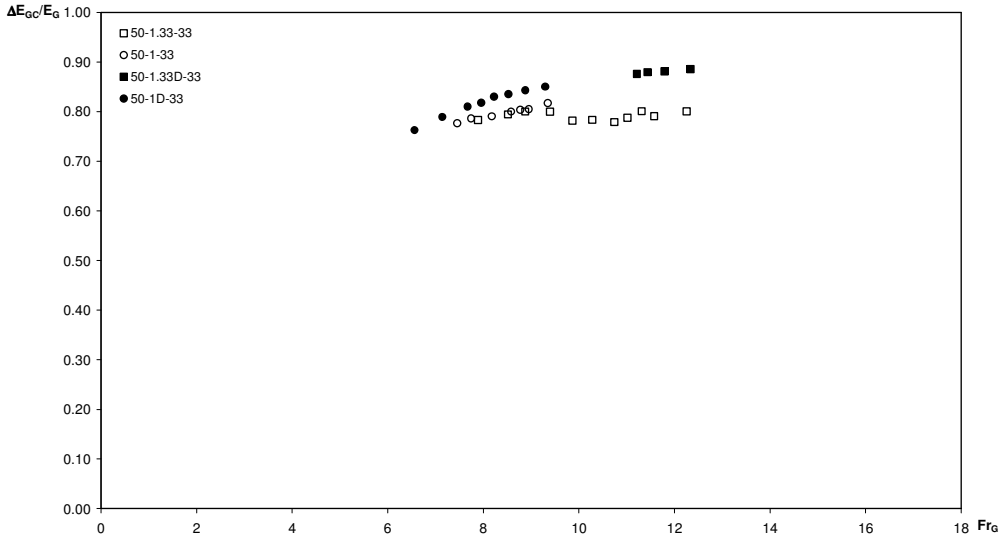

Figure 5.10 $\Delta E_{GC}/E_G$ vs. Fr_G for p=50% at X/d=33 for the comparison of single and double screens

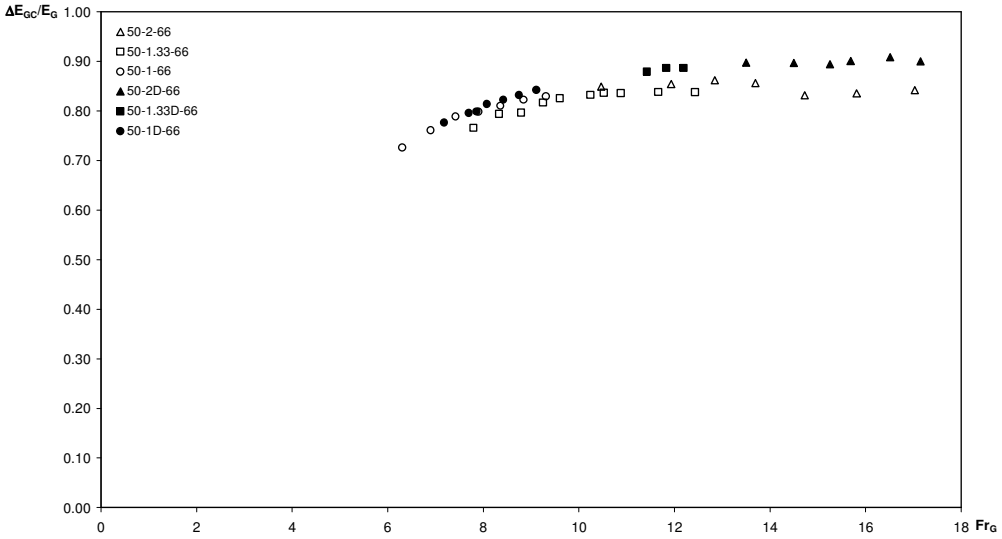

Figure 5.11 $\Delta E_{GC}/E_G$ vs. Fr_G for p=50% at X/d=66 for the comparison of single and double screens

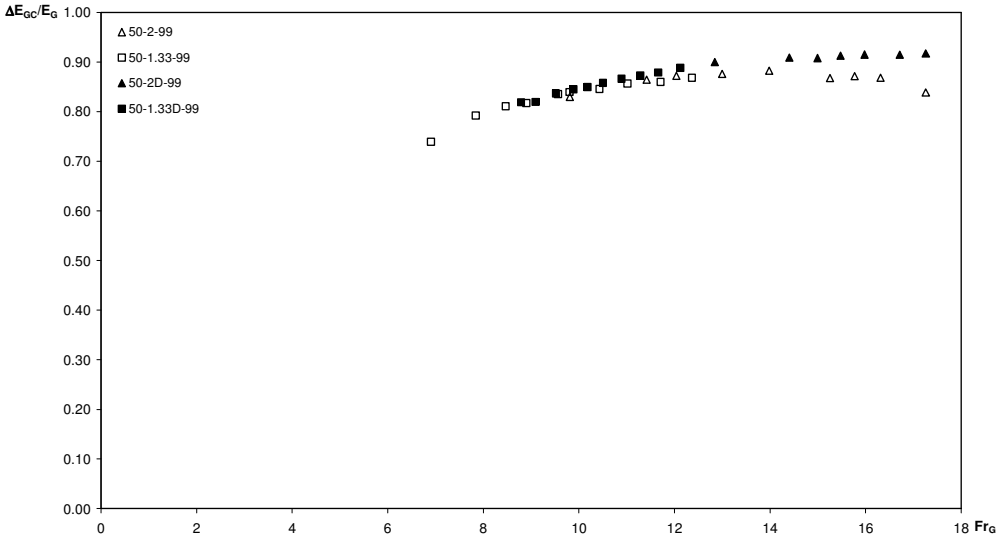

Figure 5.12 $\Delta E_{GC}/E_G$ vs. Fr_G for p=50% at X/d=99 for the comparison of single and double screens

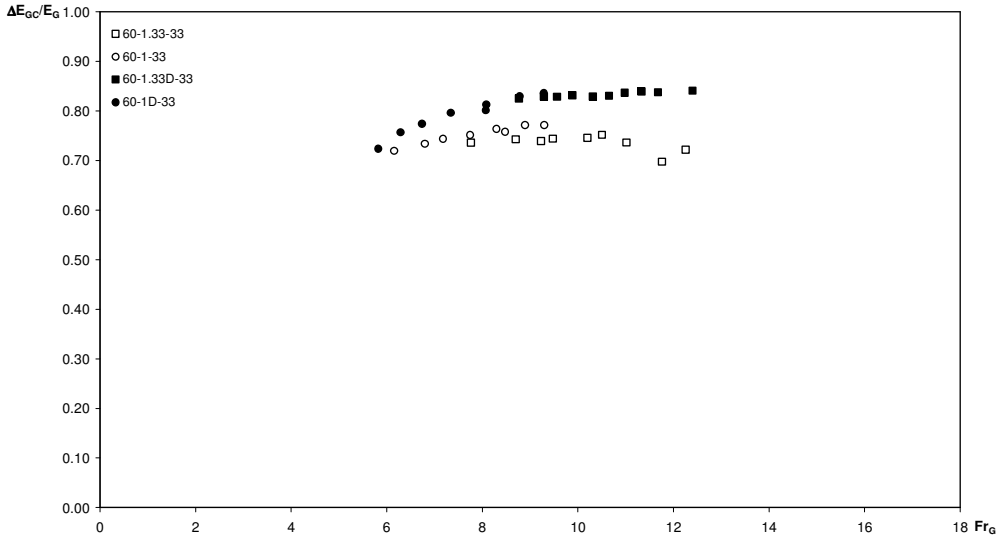

Figure 5.13 $\Delta E_{GC}/E_G$ vs. Fr_G for p=60% at X/d=33 for the comparison of single and double screens

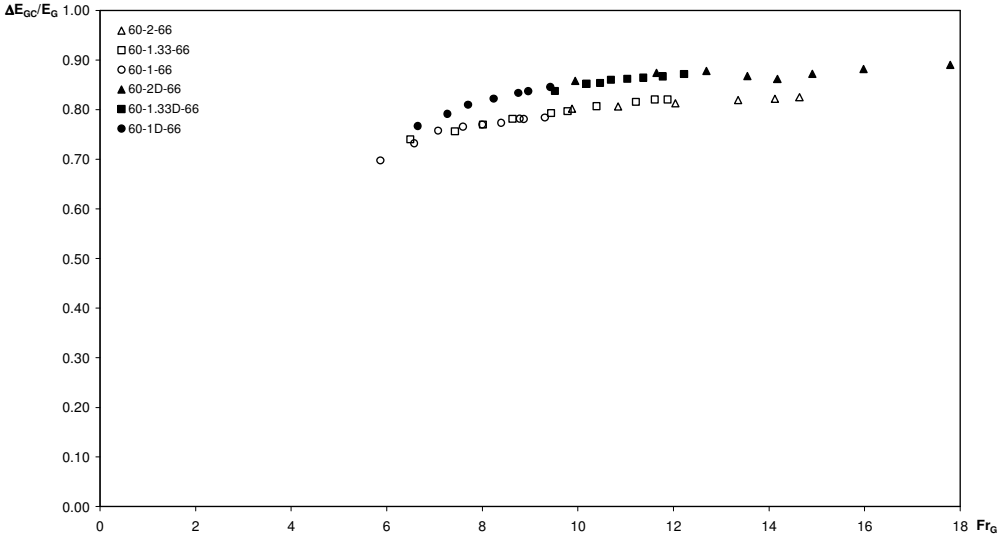

Figure 5.14 $\Delta E_{GC}/E_G$ vs. Fr_G for p=60% at X/d=66 for the comparison of single and double screens

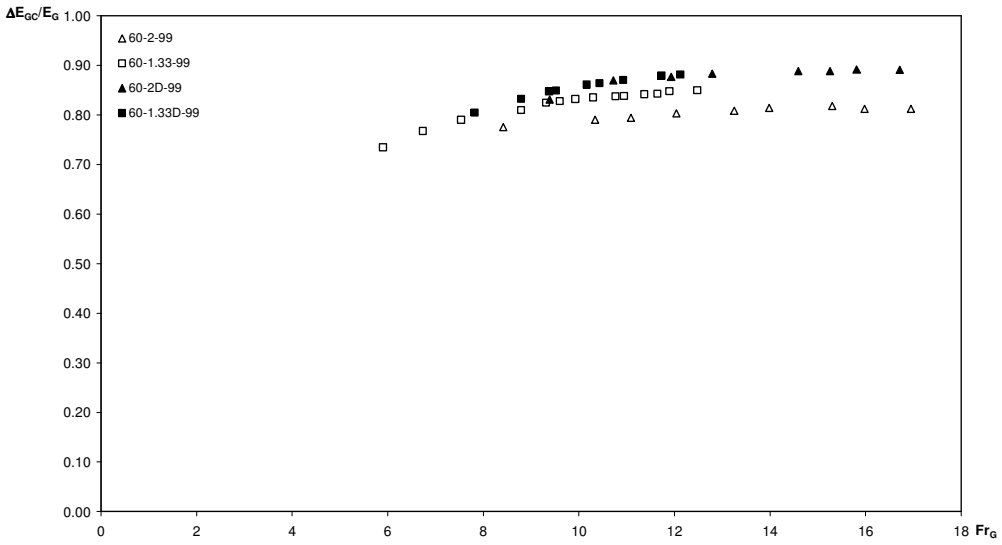

Figure 5.15 $\Delta E_{GC}/E_G$ vs. Fr_G for p=60% at X/d=99 for the comparison of single and double screens

5.3. Performance of the screens

As indicated before the energy loss through the screens are denoted as *S*. The relative energy loss S/E_G is used to analyze the performance of the screens.

5.3.1. Performance of the screens at large

The variation of the screen performance, dissipation provided by the screen, S/E_G with Fr_G is shown in figures 5.16, 5.17, 5.18, 5.19, 5.20 and 5.21 both for single and double screens.

From the examination of the figures one may discern that

i. There is an optimum range of porosity for each *X/d* for which S/E_G is maximum for single screens. Yet, within the limits of the experiments,

such dependence is not discernable for double screens.

ii. S/E_G decreases with increasing X/d.

iii. There is a very weak dependence of S/E_G on t/d for both single and double screens.

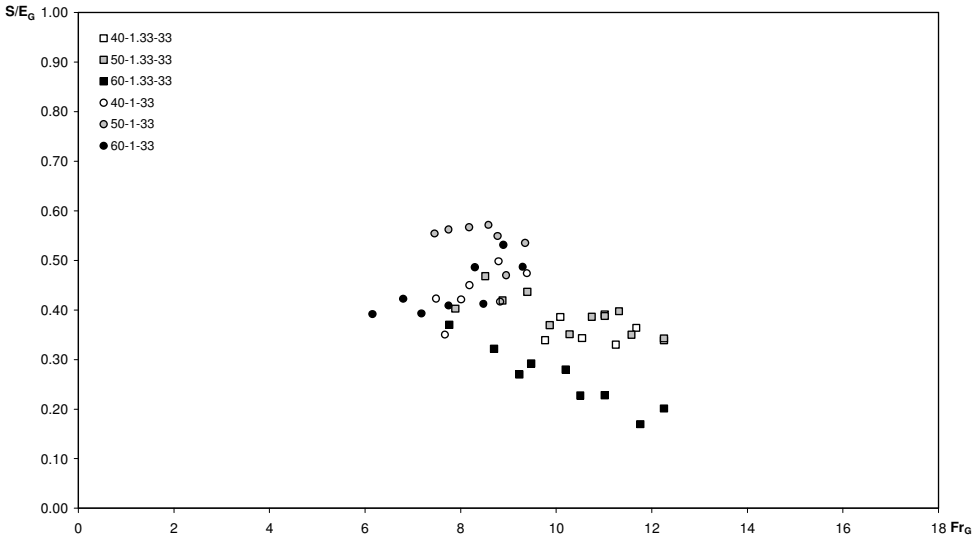

Figure 5.16 S/E_G vs. Fr_G for single screens at X/d=33

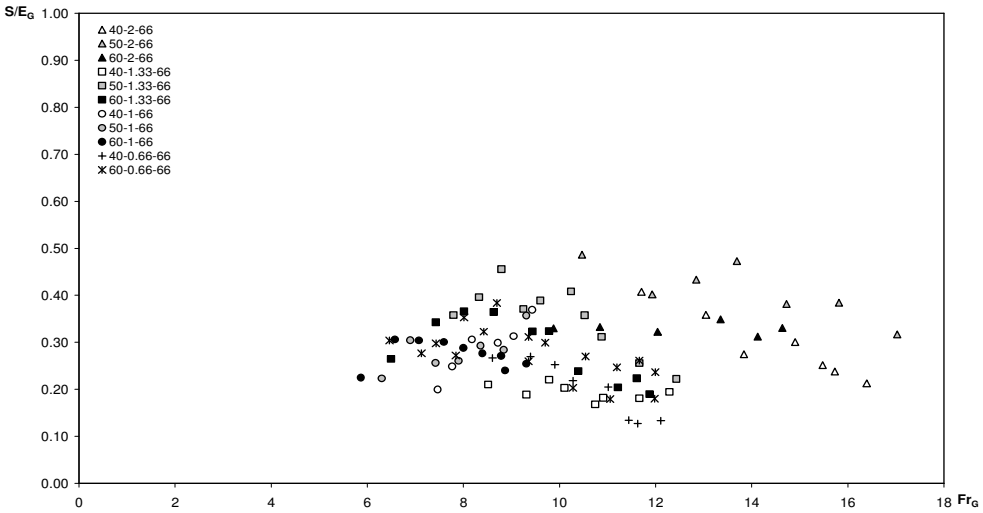

Figure 5.17 S/E_G vs. Fr_G for single screens at X/d=66

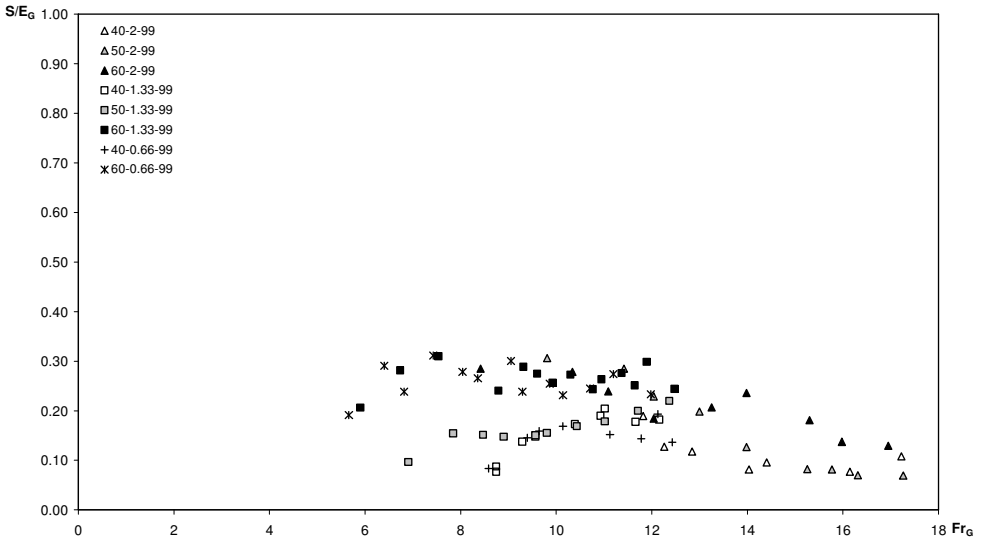

Figure 5.18 S/E_G vs. Fr_G for single screens at X/d=99

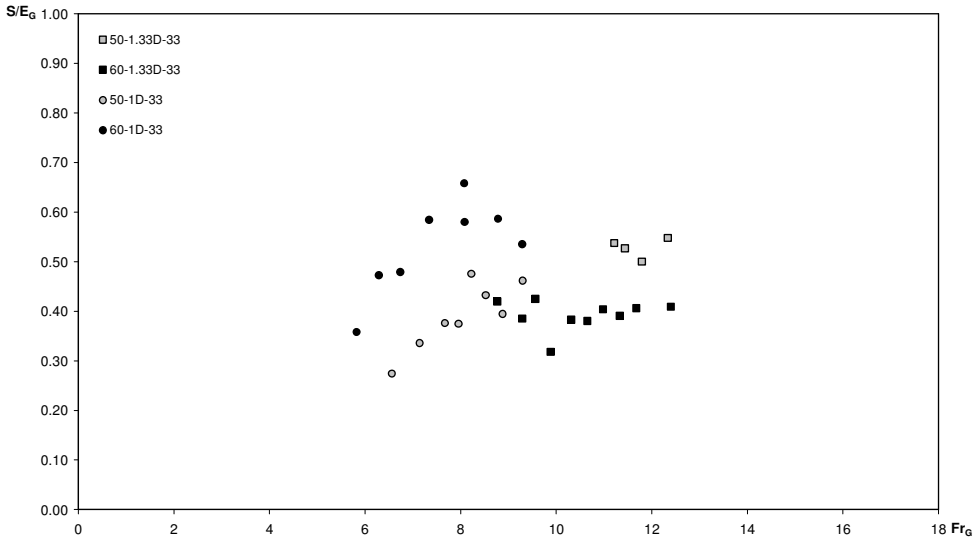

Figure 5.19 S/E_G vs. Fr_G for double screens at X/d=33

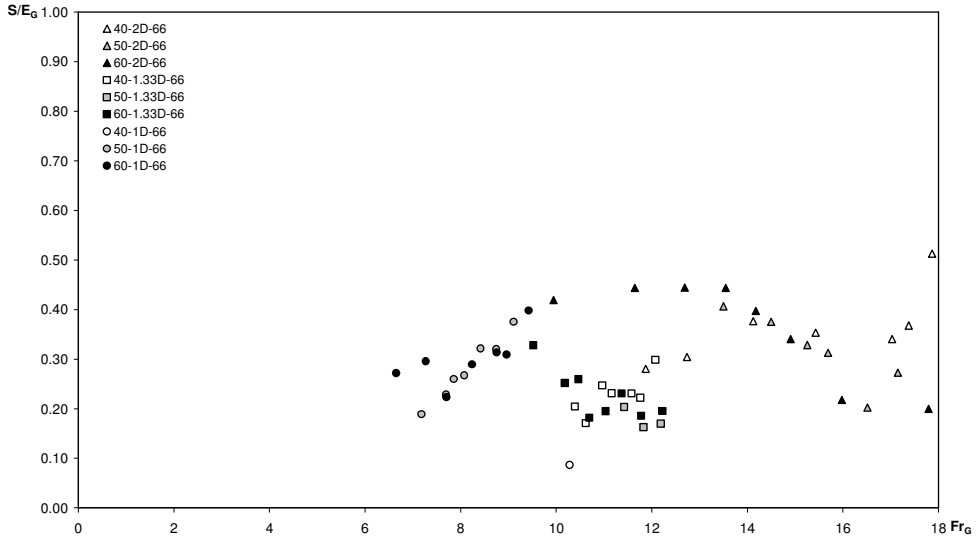

Figure 5.20 S/E_G vs. Fr_G for double screens at X/d=66

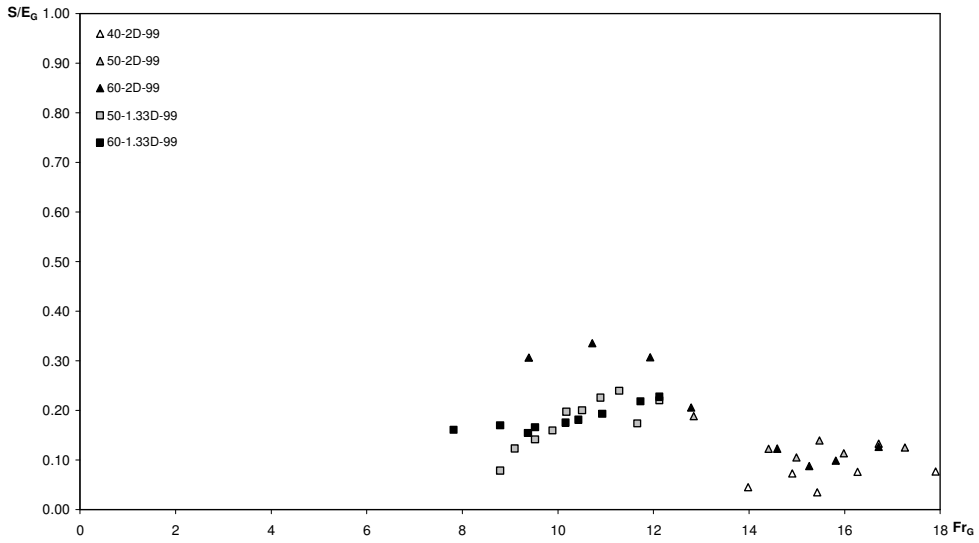

Figure 5.21 S/E_G vs. Fr_G for double screens at X/d=99

5.3.2. Comparison of screen performances of single and double screens

The screen performances for single and double screens are summarized in a graphical form in figures 5.22, 5.23, 5.24, 5.25, 5.26, 5.27, 5.28 and 5.29. From the examination of the figures no significant difference between the performances were revealed. Therefore it is concluded that for the same *X/d* and *p* values ΔE_{AB} of double screens are relatively larger than that of single screens.

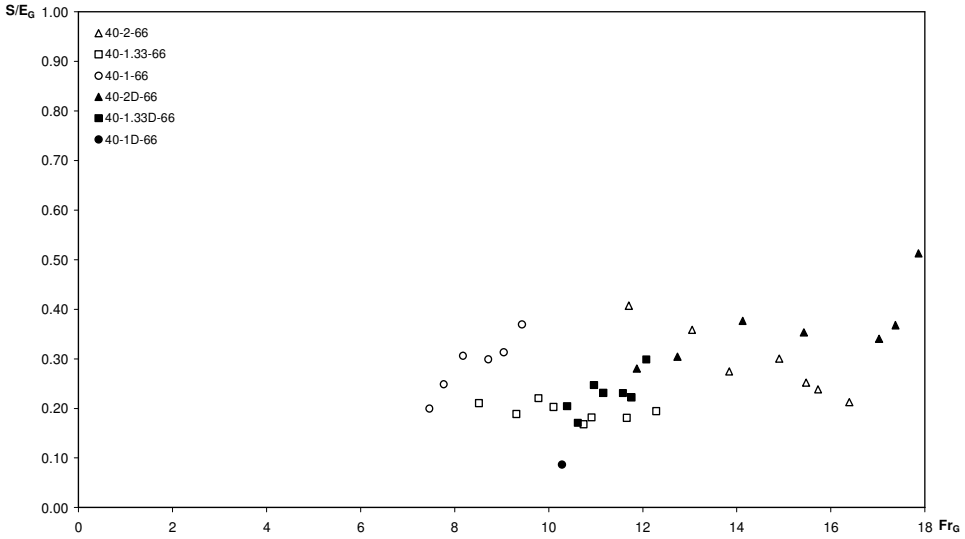

Figure 5.22 S/E_G vs. Fr_G for p=40% at X/d=66 for the comparison of single and double screens

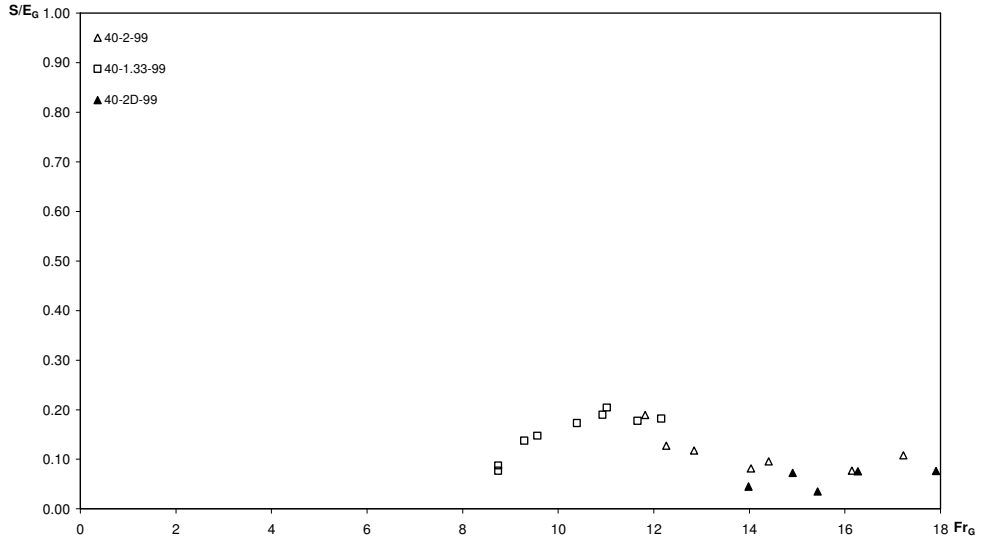

Figure 5.23 S/E_G vs. Fr_G for p=40% at X/d=99 for the comparison of single and double screens

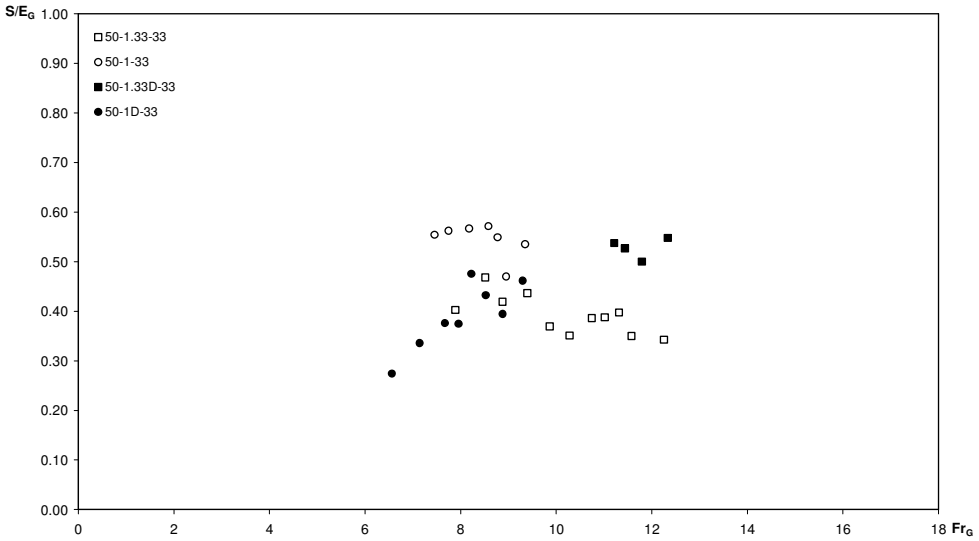

Figure 5.24 S/E_G vs. Fr_G for p=50% at X/d=33 for the comparison of single and double screens

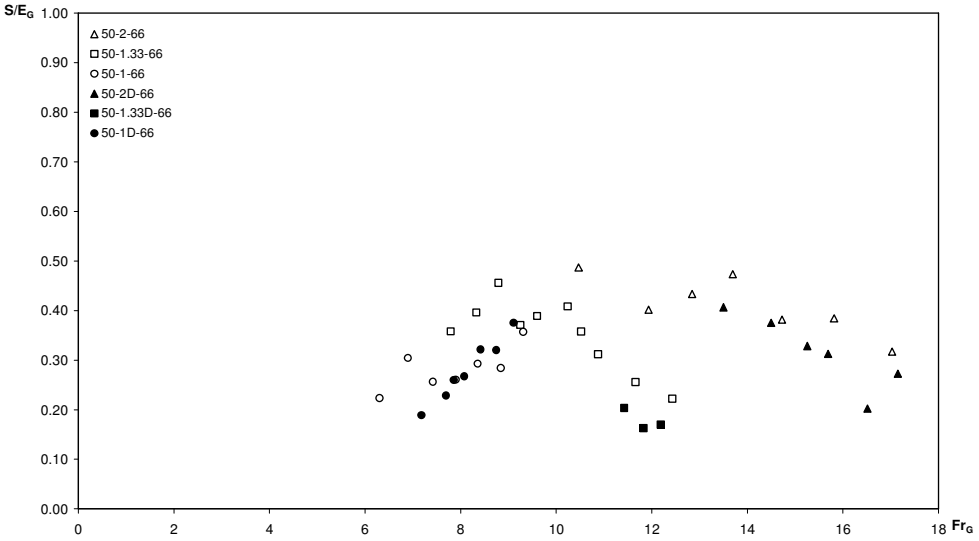

Figure 5.25 S/E_G vs. Fr_G for p=50% at X/d=66 for the comparison of single and double screens

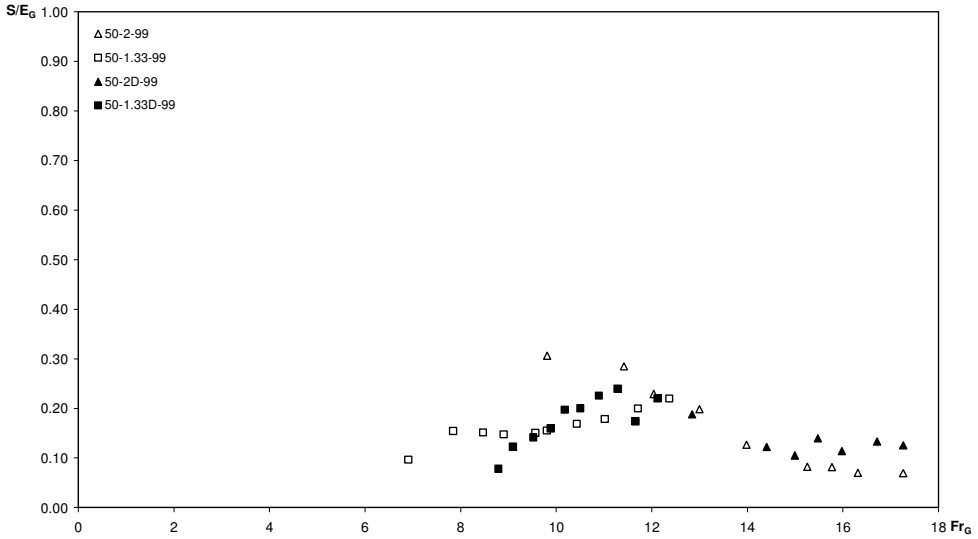

Figure 5.26 S/E_G vs. Fr_G for p=50% at X/d=99 for the comparison of single and double screens

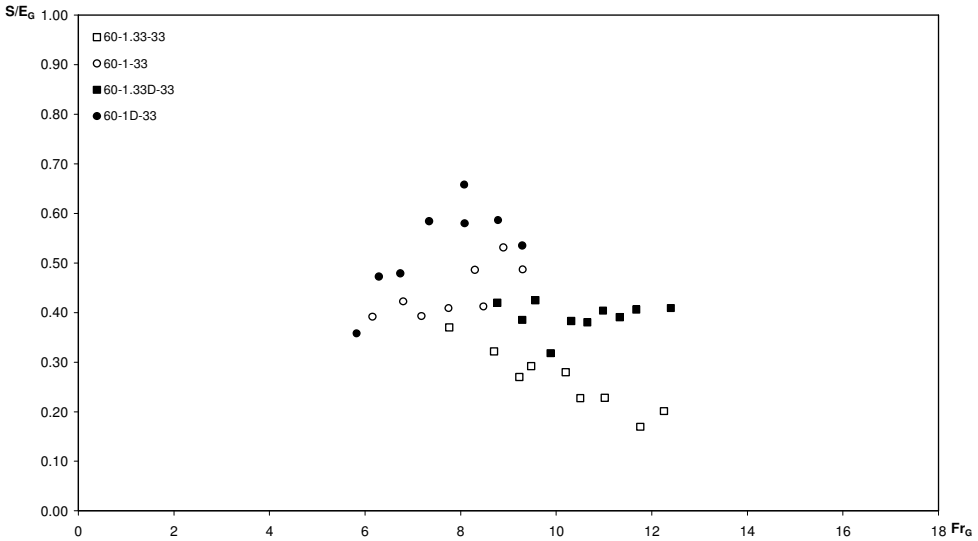

Figure 5.27 S/E_G vs. Fr_G for p=60% at X/d=33 for the comparison of single and double screens

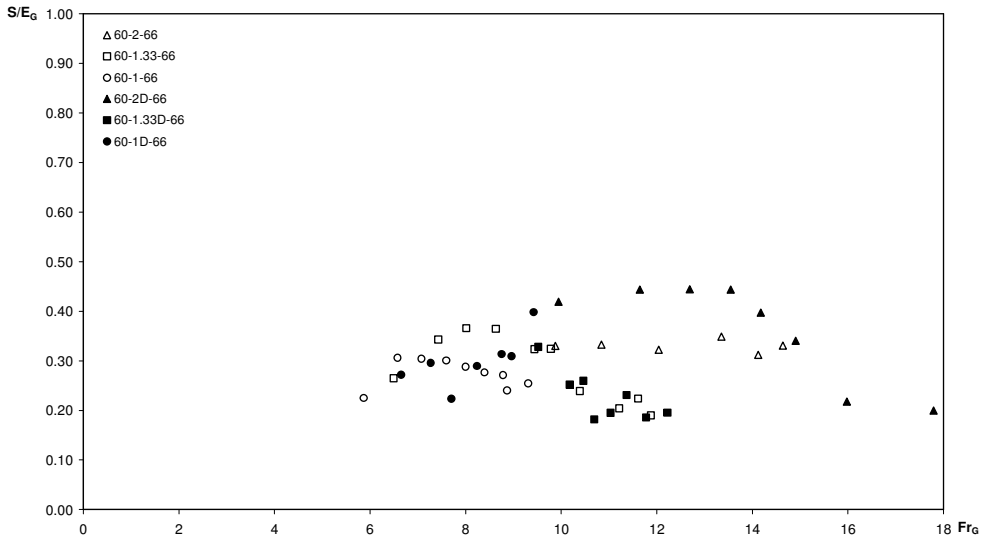

Figure 5.28 S/E_G vs. Fr_G for p=60% at X/d=66 for the comparison of single and double screens

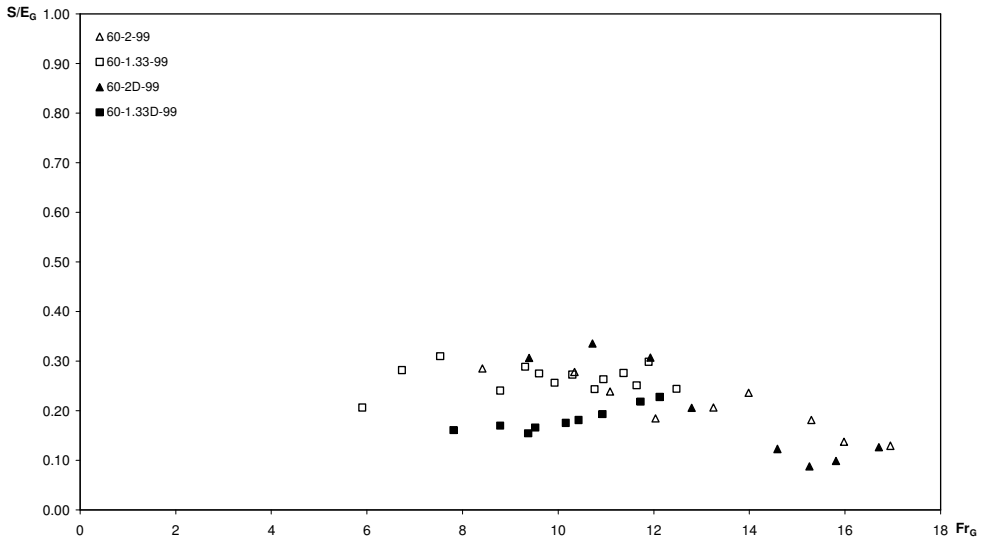

Figure 5.29 S/E_G vs. Fr_G for p=60% at X/d=99 for the comparison of single and double screens

5.4. System efficiencies

The system efficiency was defined as

$$\eta_{sys} = \frac{\Delta E_{GC} - \Delta E_{jG}}{\Delta E_{jG}} \tag{3.10}$$

In other words system efficiency is the ratio of the difference between the system loss and the loss through a hypothetical jump at section G to the loss through the hypothetical jump. Therefore, this alternative interpretation of the data in terms of system loss does not posses any new information. Yet, for convenience the variation of the system efficiencies are given below in figures 5.30, 5.31, 5.32, 5.33, 5.34 and 5.35.

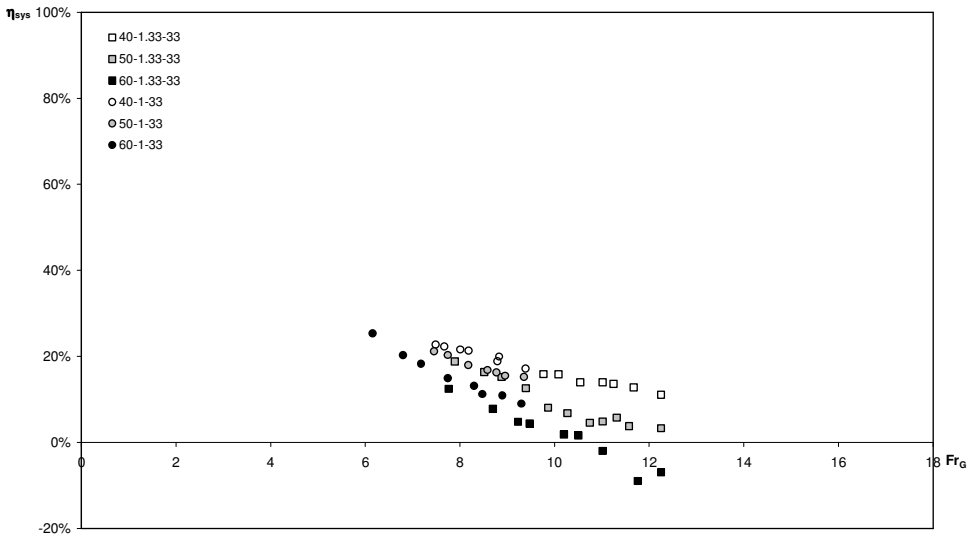

Figure 5.30 η_{sys} vs. Fr_G for single screens at X/d=33

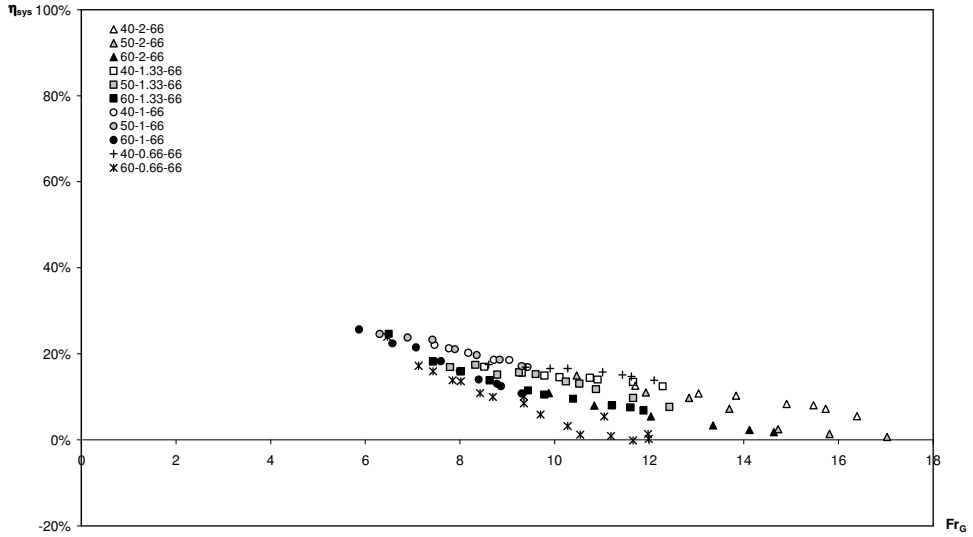

Figure 5.31 η_{sys} vs. Fr_G for single screens at X/d=66

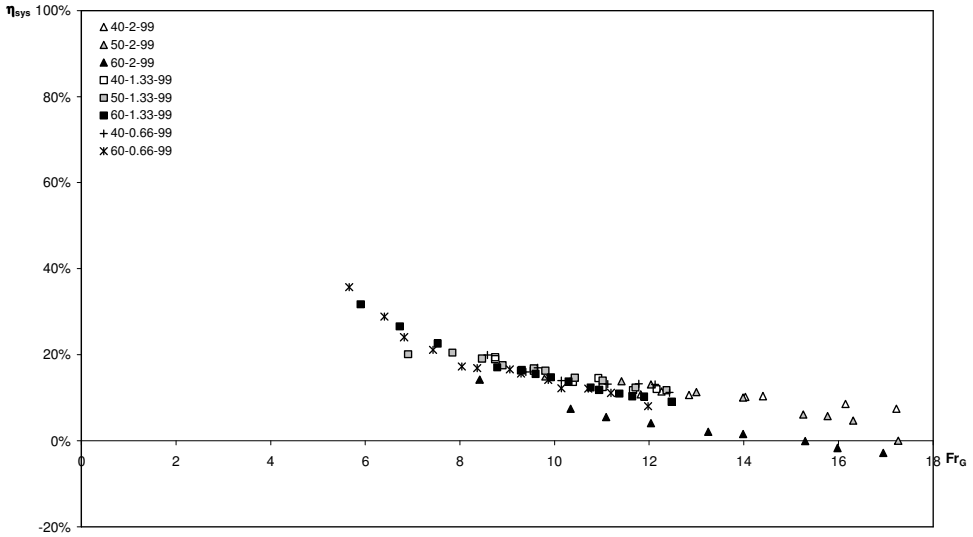

Figure 5.32 η_{sys} vs. Fr_G for single screens at X/d=99

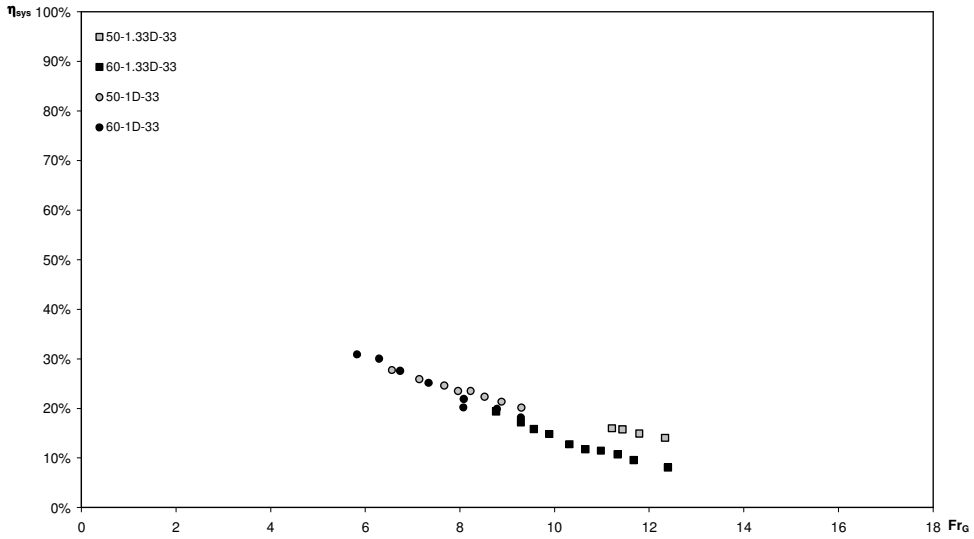

Figure 5.33 η_{sys} vs. Fr_G for double screens at X/d=33

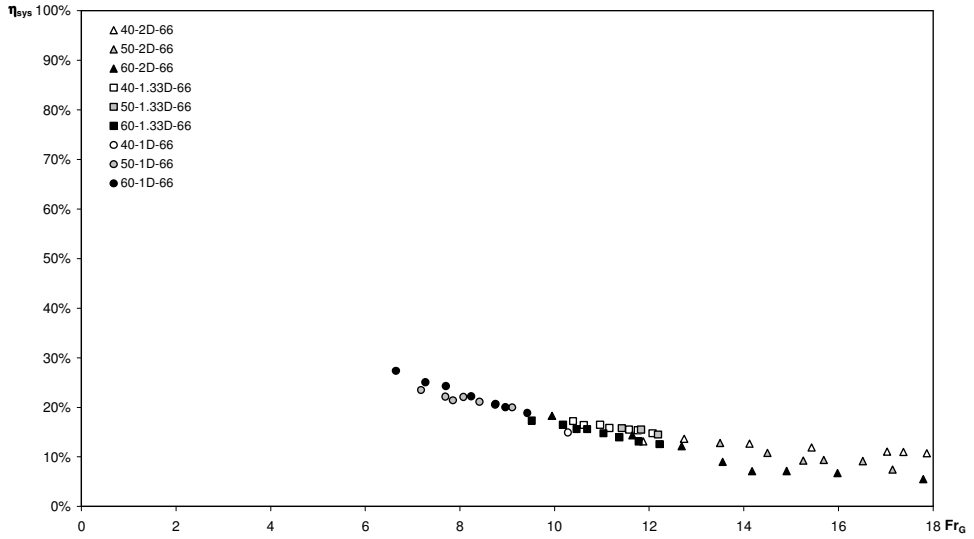

Figure 5.34 η_{sys} vs. Fr_G for double screens at X/d=66

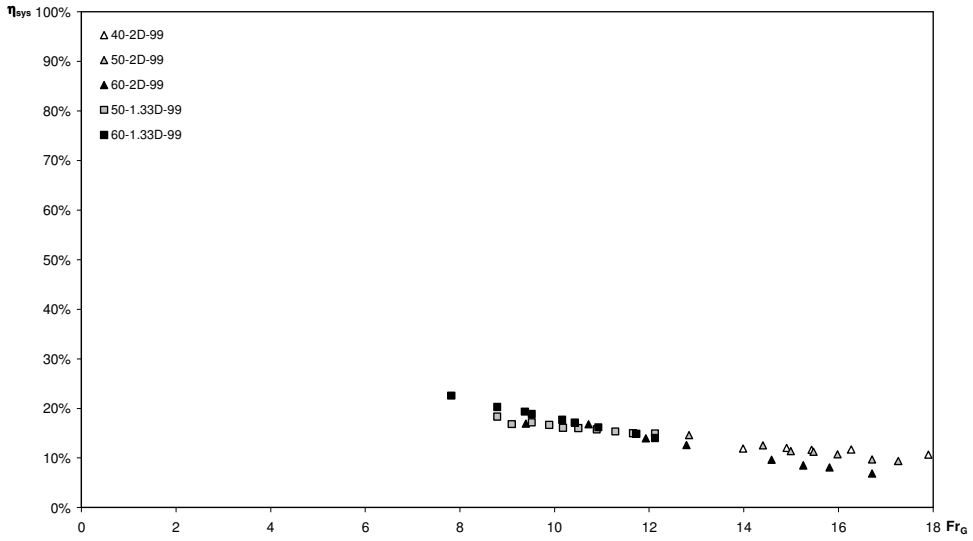

Figure 5.35 η_{sys} vs. Fr_G for double screens at X/d=99

5.5. Screen efficiencies

The screen efficiency was defined as

$$\eta_{scr} = \frac{S}{\Delta E_{jG}} \tag{3.11}$$

In other words screen efficiency is the ratio of the loss through the screen to the loss through the hypothetical jump at section G. Therefore, this alternative interpretation of the data in terms of screen loss does not posses any new information. Yet, for convenience the variation of the screen efficiencies are given below in figures 5.36, 5.37, 5.38, 5.39, 5.40 and 5.41.

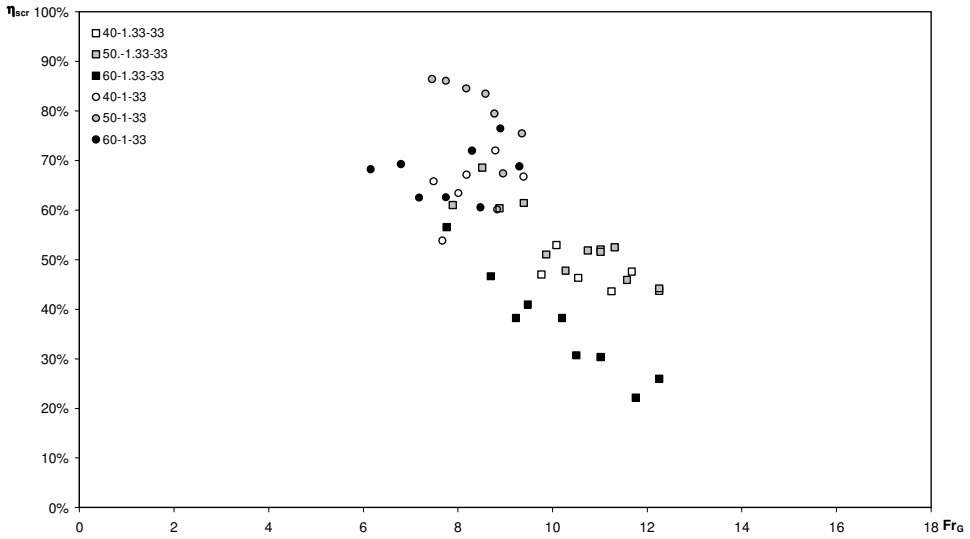

Figure 5.36 η_{scr} vs. Fr_G for single screens at X/d=33

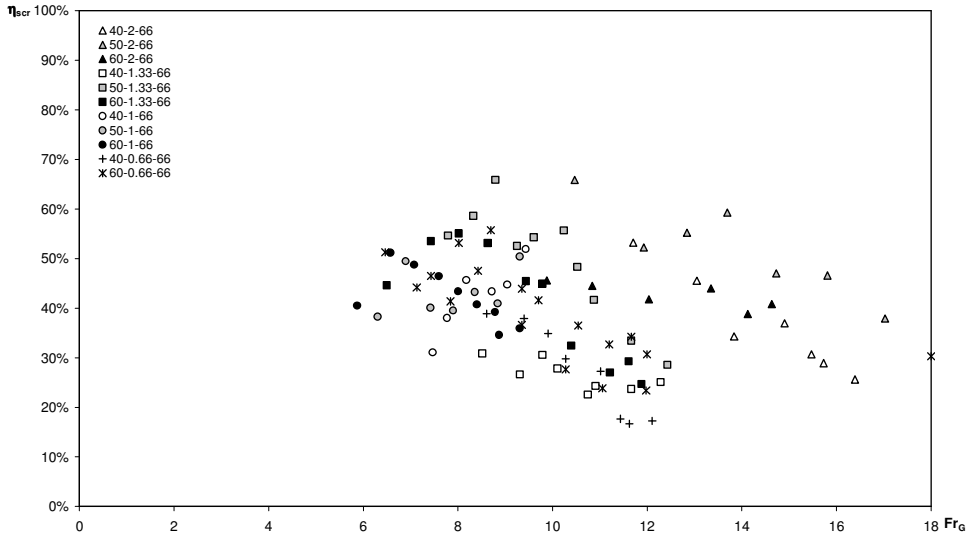

Figure 5.37 η_{scr} vs. Fr_G for single screens at X/d=66

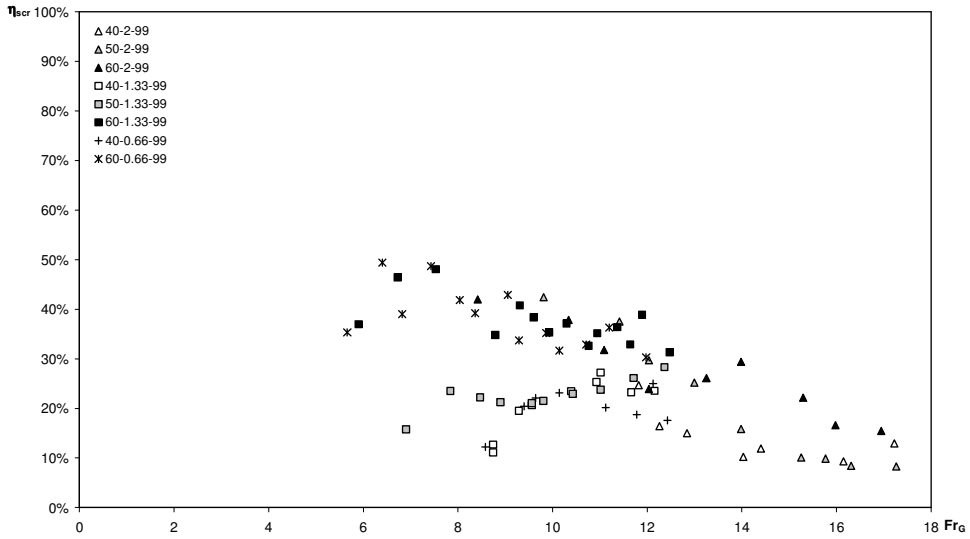

Figure 5.38 η_{scr} vs. Fr_G for single screens at X/d=99

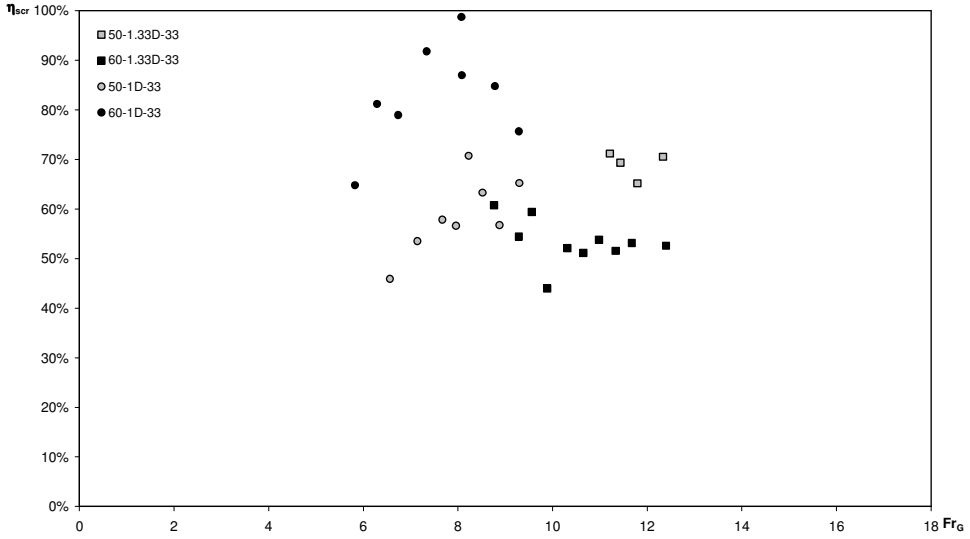

Figure 5.39 η_{scr} vs. Fr_G for double screens at X/d=33

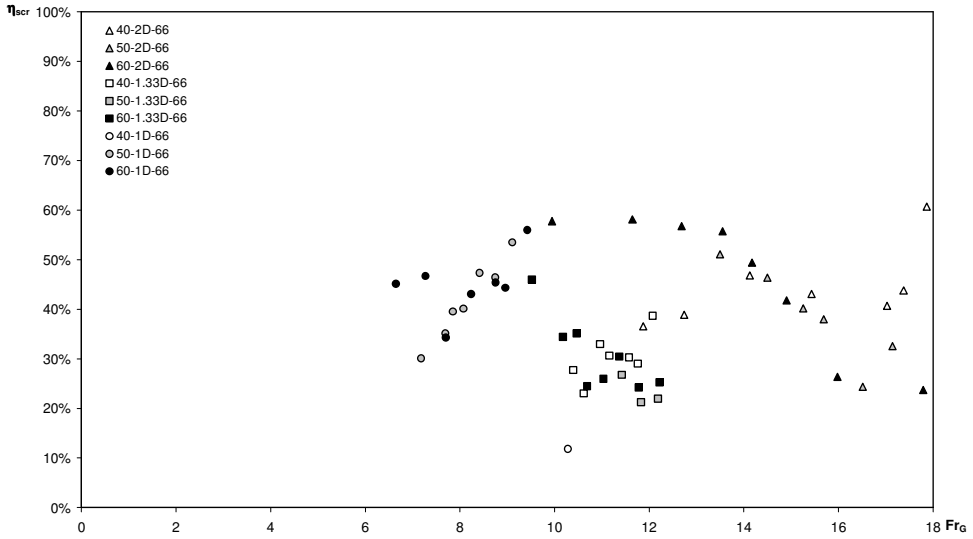

Figure 5.40 η_{scr} vs. Fr_G for double screens at X/d=66

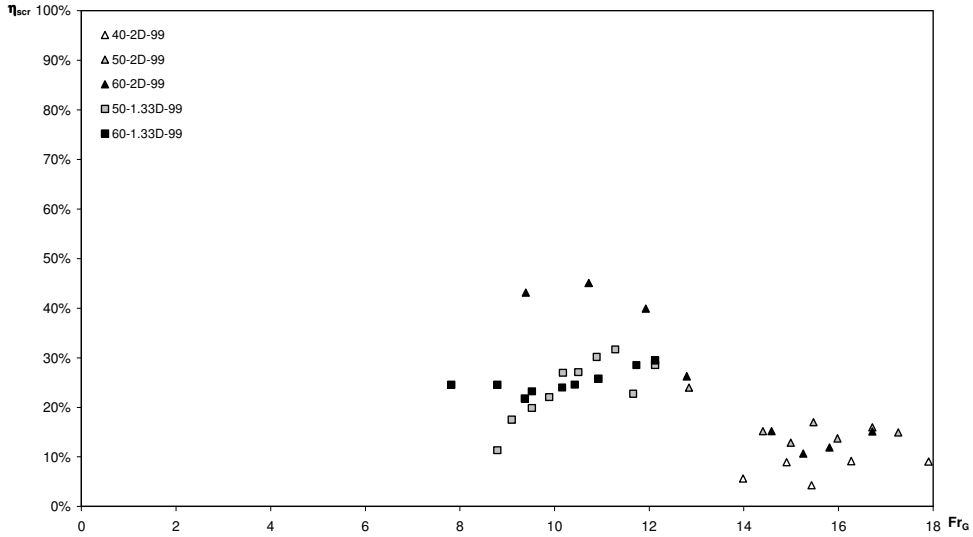

Figure 5.41 η_{scr} vs. Fr_G for double screens at X/d=99

5.6. Optimum porosities

As suggested by the data, there seems to be optimum porosities for different runs. In what follows, the variations of optimum porosities are discussed.

5.6.1. Optimum porosities for the system

The range of optimum porosities for the system for different screen positions were gathered from the data and the result thus obtained is shown in figure 5.42. The figure is drawn noting that there is no dependence of p_{opt} for the screen performance on *t/d.*

As marked in the figure, one may conclude that.

i. Both for single and double screens the range of the optimum porosity value increases with *X/d*. This implies that the system performance becomes less dependent on the porosity with increasing distance.

ii. The optimum porosities for double screens are slightly larger than the single screen at the same distance.

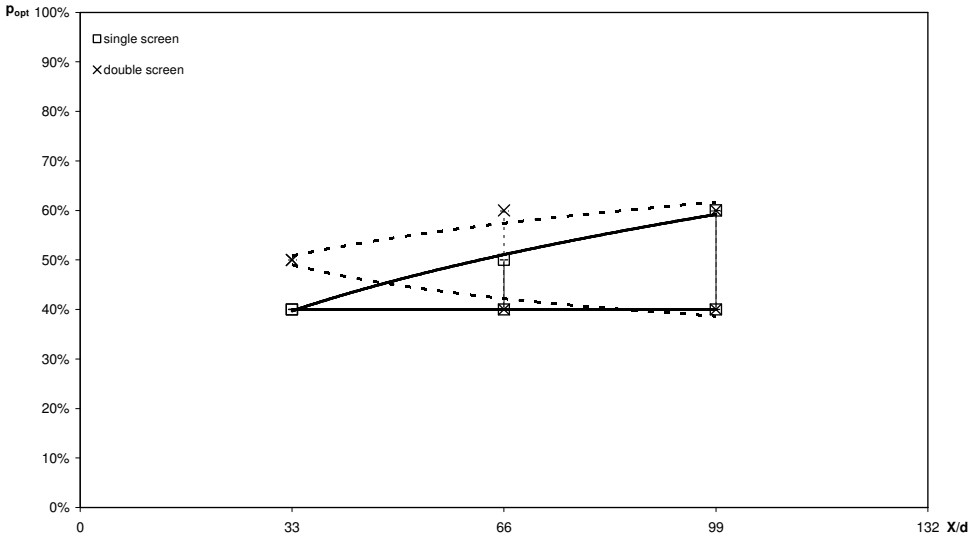

Figure 5.42 p_{opt} vs. X/d for single and double screens determined by analyzing the system efficiency

5.6.2. Optimum porosities for the screen

The range of optimum porosities for the screens for different screen positions were gathered from the data and the result thus obtained is shown in figures 5.43, 5.44 and 5.45.

From the examination of the figures 5.43 and 5.44 one may discern that

i. There is no dependence of p_{opt} for the screen performance on *t/d*. This observation is congruent with the previous observations made for the system performance above.

ii. There seems to be dependence of optimum porosity on the position of the screen for single screens such that optimum porosity increases with *X/d*. No appreciable trend of the kind is discernable for double screens.

As marked in figure 5.45, one may conclude that

i. The range of the optimum porosities decreases with increasing *X/d* for both single and double screens. Yet, double screens have a wider range.

ii. The optimum porosity slightly increases with increasing *X/d* for single screens. A very weak dependence of the same trend is suggested for double screens.

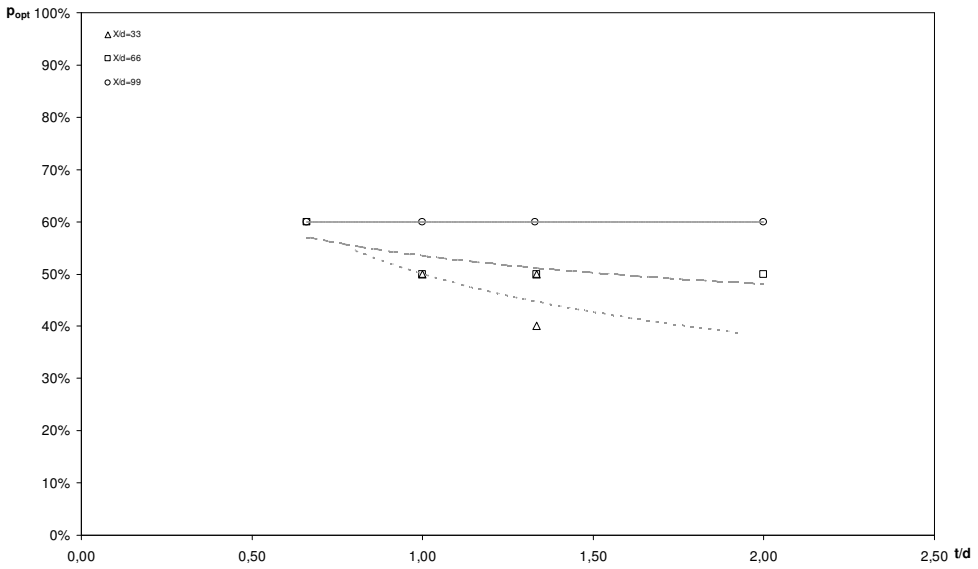

Figure 5.43 p_{opt} vs. t/d for single screens determined by analyzing the screen efficiency

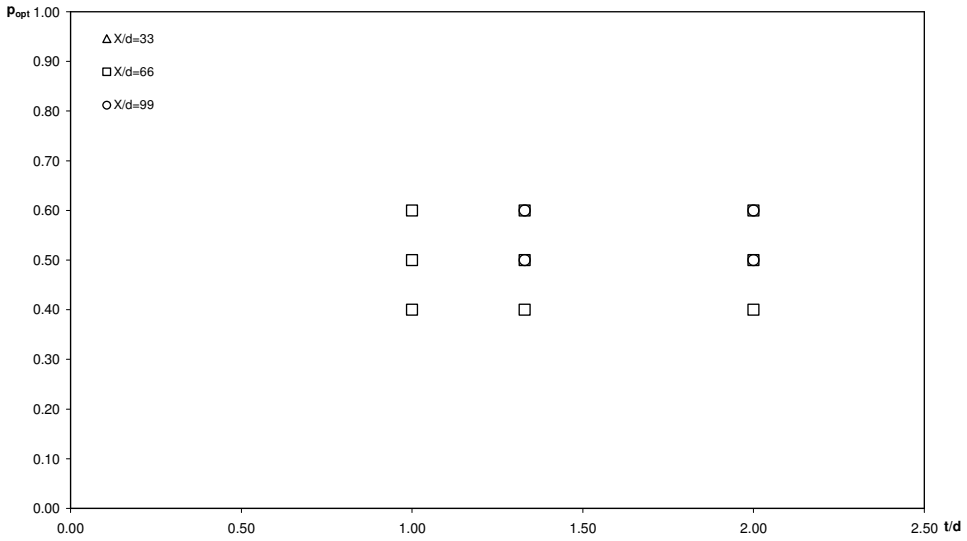

Figure 5.44 p_{opt} vs. t/d for double screens determined by analyzing the screen efficiency

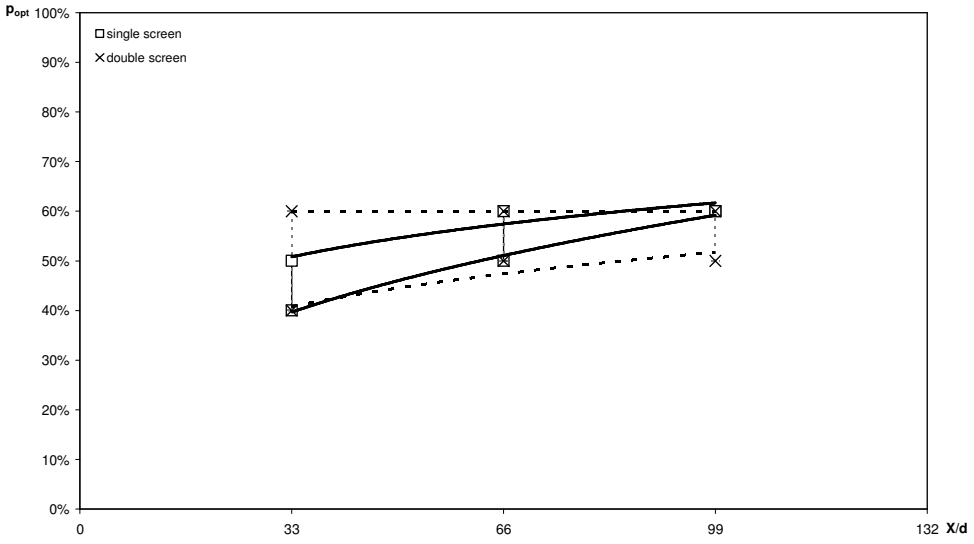

Figure 5.45 p_{opt} vs. X/d for single and double screens determined by analyzing the screen efficiency

5.7. Comparison of single and double screens system performance for optimum condition

The variations of the system performance for optimum porosities with Fr_G is given in figure 5.46. As is seen from this figure, the system performance of a double screen in general larger than that of a single screen and increases with increasing Fr_G.

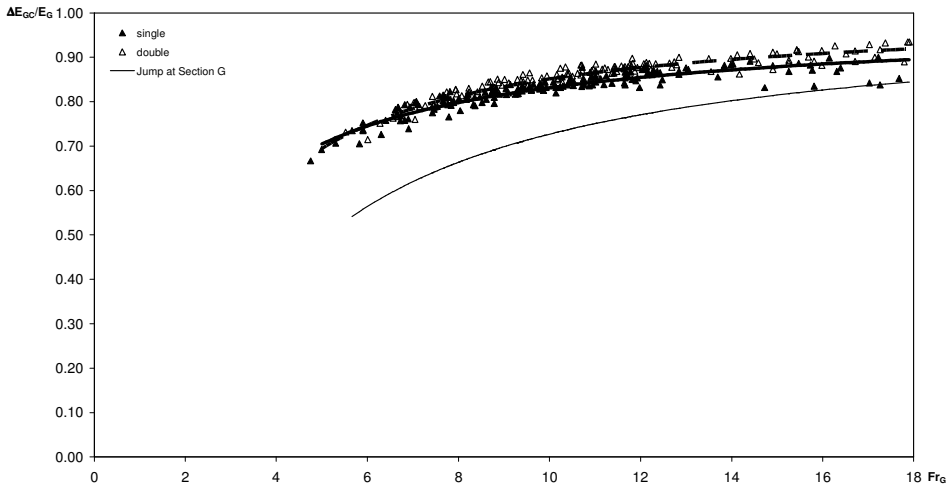

Figure 5.46 Comparison of the optimum porosities of single and double screens

CHAPTER VI

CONCLUSIONS AND RECOMMENDATIONS

In this thesis, energy dissipation performances of the screens which are efficient means of dissipating excess energy were investigated conducting a series of experiments. The experiments covered a range of Froude numbers between 5 and 18, porosities between 20% and 60%, and location of the screen up to 100 times of the undisturbed upstream flow depth.

It should be noted that while analyzing the results of the experiments, the screen performance and the system performance were investigated separately. However, the system as a whole should be the basis for design purposes.

The conclusions drawn from the analysis of the data are as follows;

- Performance of the screens ($\Delta E_{GC}/E_G$) increase with increase in Froude number while efficiency of the system (η_{sys}) decrease,

- There is an optimum range of porosities for each *X/d*. However, p=40% provides generally higher energy dissipation,

- Since the range of optimum porosities enlarges as *X/d* increases, the question of "which value of the porosity should be selected" looses its

importance,

- Performance and efficiency of the screens decrease with increase in *X/d* values,

- Yet, for small *X/d* values (e.g. about 33) screens of 40% porosity or less would cause chocking of the outlet,

- There is no dependence of p_{opt} on *t/d* considering the energy dissipating performance of the system within the range covered,

- Double screens dissipate more energy than single screens. But, the decision about the type of screen depends on the results of the feasibility studies.

A screen located at a proper location can work efficiently for a very wide range of Froude numbers. However, a stilling basin is designed for a specific discharge value. Furthermore, screens are more effective than a hydraulic jump to dissipate energy. Therefore, it is recommended that the present study be investigated further by taking into account the following;

- thicker screens,

- multiple screens,

- inclined screens,

- screens of different porosity values with a wider range and finer increments,

- a wider range of screen positioning with finer screens, or

- different hole geometry.

The results obtained from this study can be utilized efficiently in practice. However, it should be noted that prior to the application of screen structures, several investigations should be performed. These investigations should cover the real life factors like vibration of the structure or accumulation of debris behind the screen that could cause blockage of the holes.

REFERENCES

Baines, W. D., Peterson, E. G. (1951). "An Investigation of Flow Through Screens." Transactions of the ASME, Vol. 73, No. 5, 467-480

French, R. H. (1986). "Open Channel Hydraulics." McGraw-Hill Book Company, Singapore.

Koo, J. K., James, D. F. (1973). "Fluid Flow Around and Through a Screen." Journal of Fluid Mechanics, Vol. 60, Part 3, 513-538

Laws, E. M., Livesey, J. L. (1978). "Flow Through Screens." Annual Reviews of Fluid Mechanics, Vol. 10, 247-266

Manson, B.R., Young, D. F. and Okiishi, T. H. (1994). "Fundamentals of Fluid Mechanics." John Wiley and Sons, Inc., Toronto, Canada.

Rajaratnam, N., Hurtig, K. I. (2000). "Screen-Type Energy Dissipator for Hydraulic Structures." Journal of Hydraulic Engineering, Vol. 126, No. 4, 310-312

Simon, A. L. (1981). "Practical Hydraulics." John Wiley and Sons, Inc., Toronto, Canada.

Yeh, H. H., Shrestha, M. (1989). "Free-Surface Flow Through Screen." Journal of Hydraulic Engineering, Vol. 115, No. 10, 1371-1385

APPENDIX A

ORIFICE METER DETAILS

In the experimental setup, $\phi = 0.5$ is chosen and it is defined as $\phi = \frac{D_0}{D_1}$

where D_0 is the orifice meter throat diameter and D_1 is the pipe diameter on which the orifice meter located.

All other parameters are arranged implementing the requirements given in TSE (figure A.1).

The principle of the orifice is based on that reduction of the cross section of the flowing stream in passing through the orifice causes an increase in velocity that is accompanied by a decrease in pressure and the reduction in pressure between the taps is measured by the manometer. Bernoulli's equation provides a basis for correlating the increase in velocity head with the decrease in pressure head and this correlation provides a way of measuring the flowrate (*Manson, Young, and Okiishi (1994)).*

If it is assumed that the flow is horizontal, steady, inviscid and incompressible between points (1) and (2), Bernoulli equation becomes

$$\frac{p_1}{\gamma}+\frac{V_1^{\,2}}{2g}=\frac{p_2}{\gamma}+\frac{V_2^{\,2}}{2g}+h_L \tag{A.1}$$

The ideal situation has $h_L=0$. Non-ideal effects occur for two reasons. First, the vena contracta area, A_2, is less than the area of the hole, A_0, by an unknown amount. Thus, $A_2=C_cA_0$, where C_c is the contraction coefficient (C_c<1). Second, the swirling flow and turbulent motion near the orifice plate introduce a head loss that cannot be calculated theoretically. As a result, an orifice discharge coefficient, C_0, is used to take these effects into account. That is,

$$Q=C_0Q_{ideal}=C_0A_0\sqrt{\frac{2(p_1-p_2)}{\rho(1-\phi^4)}} \tag{A.2}$$

where $A_0=\frac{\pi D_0^{\,2}}{4}$ is the area of the hole in the orifice plate. The value of C_0 is a function of $\phi=\frac{D_0}{D_1}$ and the Reynolds number $Re=\frac{\rho V_1D_1}{\mu}$, where $V_1=\frac{Q}{A_1}$. The value of C_0 depends on the specific construction of the orifice meter.

For the determination of C_0 coefficient, the distinct values given by TSE are used here by fitting a proper trend curve for the discharge calculations (figure A.2).And all the details of the orifice-meter are given in figure A.1.

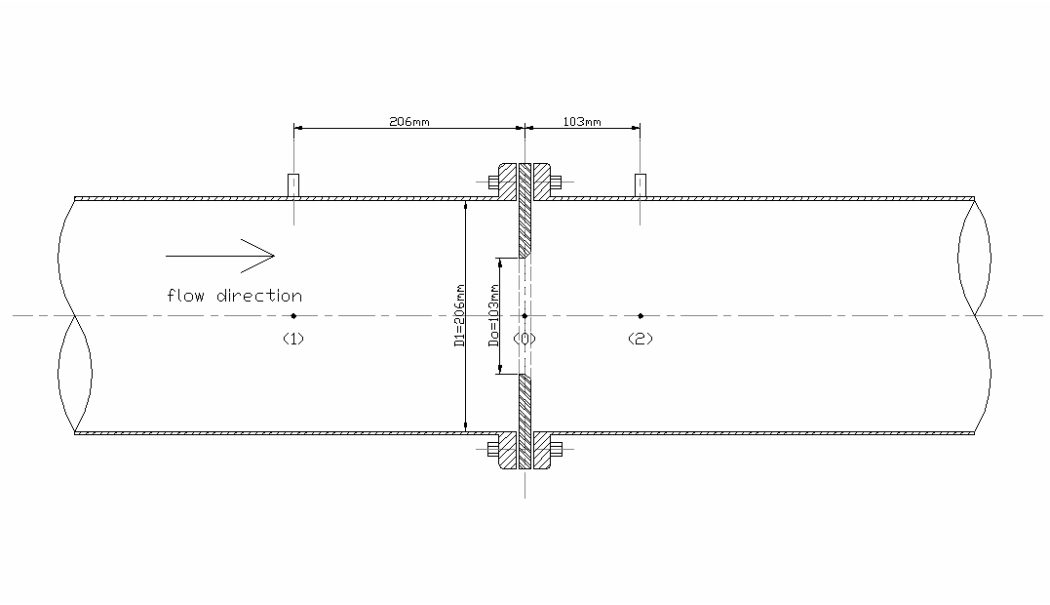

Figure A.1 Details of the orifice-meter

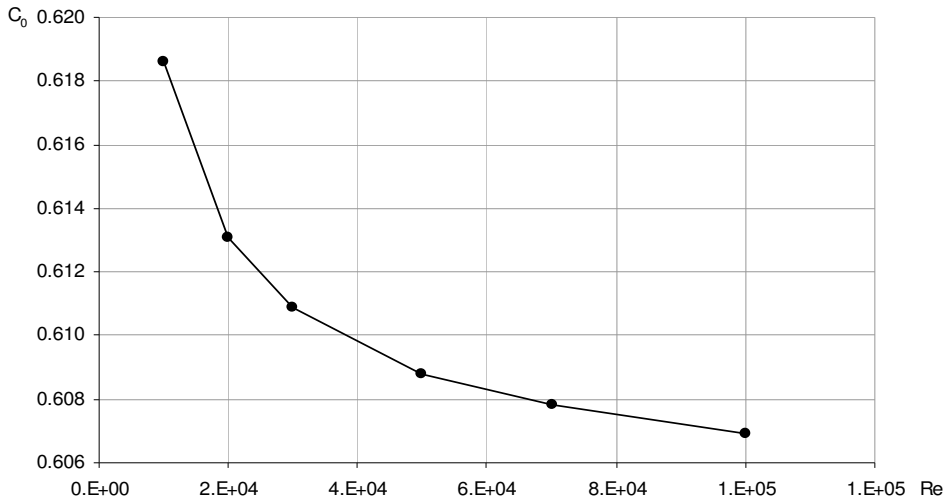

Figure A.2 C_0 vs. *Re* graph for the orifice-meter

APPENDIX B

EXPERIMENTAL DATA

The measurements made are given in table B.1 below.

Table B.1 Experimental Data

Reference	***Q (m^3/s)***	***y_C (cm)***	***y_A (cm)***
60-0.66-66-11.99	0.025	3.73	2.50
60-0.66-66-11.98	0.025	3.82	2.71
60-0.66-66-11.66	0.024	3.65	2.41
60-0.66-66-11.19	0.023	3.66	2.45
60-0.66-66-11.05	0.023	4.01	2.77
60-0.66-66-10.54	0.022	3.58	2.36
60-0.66-66-10.28	0.021	3.67	2.57
60-0.66-66-9.71	0.020	3.75	2.32
60-0.66-66-9.35	0.020	3.87	2.32
60-0.66-66-9.35	0.020	4.01	2.48
60-0.66-66-8.7	0.018	3.80	2.15
60-0.66-66-8.42	0.018	3.79	2.26
60-0.66-66-8.01	0.017	3.87	2.21
60-0.66-66-7.84	0.016	3.82	2.37
60-0.66-66-7.43	0.016	3.82	2.30
60-0.66-66-7.13	0.015	3.79	2.34
60-0.66-66-6.46	0.014	3.99	2.29
60-0.66-99-11.98	0.025	4.55	2.70
60-0.66-99-11.19	0.023	4.79	2.58
60-0.66-99-10.71	0.022	4.77	2.67
60-0.66-99-10.14	0.021	4.55	2.68
60-0.66-99-9.87	0.021	4.74	2.62

Table B.1 Experimental Data continued

Reference	*Q (m^3/s)*	*y_C (cm)*	*y_A (cm)*
60-0.66-99-9.29	0.019	4.69	2.66
60-0.66-99-9.05	0.019	4.73	2.46
60-0.66-99-8.36	0.017	4.37	2.49
60-0.66-99-8.04	0.017	4.24	2.43
60-0.66-99-7.43	0.016	4.36	2.34
60-0.66-99-6.82	0.014	4.28	2.49
60-0.66-99-6.4	0.013	4.58	2.34
60-0.66-99-5.66	0.012	4.83	2.45
60-1.33-99-12.48	0.026	4.87	2.72
60-1.33-99-11.89	0.025	4.90	2.54
60-1.33-99-11.64	0.024	4.82	2.68
60-1.33-99-11.37	0.024	4.83	2.59
60-1.33-99-10.95	0.023	4.82	2.63
60-1.33-99-10.76	0.023	4.84	2.70
60-1.33-99-10.3	0.022	4.88	2.59
60-1.33-99-9.93	0.021	4.89	2.64
60-1.33-99-9.6	0.020	4.86	2.57
60-1.33-99-9.31	0.019	4.86	2.52
60-1.33-99-8.79	0.018	4.64	2.63
60-1.33-99-7.53	0.016	4.67	2.37
60-1.33-99-6.73	0.014	4.58	2.39
60-1.33-99-5.9	0.012	4.40	2.40
40-1.33-99-12.16	0.025	5.41	2.81
40-1.33-99-11.66	0.024	5.12	2.76
40-1.33-99-11.02	0.023	4.97	2.59
40-1.33-99-10.93	0.023	5.43	2.70
40-1.33-99-10.39	0.022	4.92	2.60
40-1.33-99-9.56	0.020	4.98	2.64
40-1.33-99-9.29	0.019	4.82	2.57
40-1.33-99-8.74	0.018	4.98	2.65
40-1.33-99-8.74	0.018	5.08	2.66
40-0.66-99-12.43	0.026	5.32	2.93
40-0.66-99-12.12	0.025	5.73	2.69
40-0.66-99-11.78	0.025	5.57	2.88
40-0.66-99-11.12	0.023	5.18	2.79
40-0.66-99-10.14	0.021	4.85	2.64
40-0.66-99-9.64	0.020	5.20	2.69
40-0.66-99-9.4	0.020	4.82	2.67
40-0.66-99-8.58	0.018	5.07	2.75
40-1.33-66-12.29	0.026	5.61	2.92
40-1.33-66-11.66	0.024	5.56	2.95
40-1.33-66-10.91	0.023	5.28	2.86
40-1.33-66-10.75	0.022	5.28	2.92
40-1.33-66-10.1	0.021	4.94	2.68
40-1.33-66-9.79	0.020	4.84	2.58
40-1.33-66-9.31	0.019	4.70	2.59
40-1.33-66-8.52	0.018	4.48	2.42
40-0.66-66-12.11	0.025	6.01	3.02
40-0.66-66-11.63	0.024	6.00	3.08

Table B.1 Experimental Data continued

Reference	*Q (m^3/s)*	*y_C (cm)*	*y_A (cm)*
40-0.66-66-11.44	0.024	5.99	3.02
40-0.66-66-11.02	0.023	5.90	2.68
40-0.66-66-10.28	0.021	5.58	2.55
40-0.66-66-9.91	0.021	5.29	2.39
40-0.66-66-9.4	0.020	5.01	2.33
40-0.66-66-8.61	0.018	4.60	2.23
60-1.33-66-11.88	0.025	4.36	2.83
60-1.33-66-11.61	0.024	4.38	2.70
60-1.33-66-11.21	0.023	4.34	2.76
60-1.33-66-10.39	0.022	4.28	2.61
60-1.33-66-9.79	0.020	4.20	2.35
60-1.33-66-9.44	0.020	4.19	2.34
60-1.33-66-8.63	0.018	4.14	2.23
60-1.33-66-8.01	0.017	4.08	2.21
60-1.33-66-7.43	0.016	4.02	2.23
60-1.33-66-6.49	0.014	4.09	2.39
50-1.33-66-12.43	0.026	4.62	2.75
50-1.33-66-11.66	0.024	4.72	2.64
50-1.33-66-10.87	0.023	4.78	2.46
50-1.33-66-10.52	0.022	4.86	2.35
50-1.33-66-10.24	0.021	4.82	2.23
50-1.33-66-9.6	0.020	4.80	2.25
50-1.33-66-9.25	0.019	4.68	2.26
50-1.33-66-8.79	0.018	4.36	2.07
50-1.33-66-8.33	0.017	4.43	2.16
50-1.33-66-7.79	0.016	4.08	2.17
50-1.33-99-12.37	0.026	5.44	2.85
50-1.33-99-11.71	0.024	5.29	2.90
50-1.33-99-11.02	0.023	5.34	2.98
50-1.33-99-10.43	0.022	5.14	2.97
50-1.33-99-9.81	0.021	5.14	3.00
50-1.33-99-9.56	0.020	5.10	3.01
50-1.33-99-8.9	0.019	4.80	2.92
50-1.33-99-8.47	0.018	4.79	2.87
50-1.33-99-7.84	0.016	4.56	2.76
50-1.33-99-6.91	0.014	3.92	2.63
50-1.33-33-12.25	0.026	4.04	2.29
50-1.33-33-11.58	0.024	3.96	2.26
50-1.33-33-11.32	0.024	4.10	2.18
50-1.33-33-11.02	0.023	3.95	2.17
50-1.33-33-10.75	0.022	3.86	2.16
50-1.33-33-10.28	0.021	3.96	2.23
50-1.33-33-9.87	0.021	3.97	2.19
50-1.33-33-9.4	0.020	4.30	2.10
50-1.33-33-8.88	0.019	4.41	2.12
50-1.33-33-8.52	0.018	4.39	2.03
50-1.33-33-7.89	0.016	4.35	2.11
40-1.33D-66-12.08	0.025	6.42	2.12
40-1.33D-66-11.76	0.025	6.44	2.25

Table B.1 Experimental Data continued

Reference	*Q (m^3/s)*	*y_C (cm)*	*y_A (cm)*
40-1.33D-66-11.58	0.024	6.33	2.25
40-1.33D-66-11.16	0.023	6.08	2.15
40-1.33D-66-10.96	0.023	6.19	2.09
40-1.33D-66-10.62	0.022	5.83	2.21
40-1.33D-66-10.39	0.022	5.94	2.03
60-1.33D-33-12.4	0.026	4.68	2.23
60-1.33D-33-11.68	0.024	4.70	2.22
60-1.33D-33-11.33	0.024	4.78	2.26
60-1.33D-33-10.98	0.023	4.77	2.22
60-1.33D-33-10.65	0.022	4.69	2.25
60-1.33D-33-10.32	0.022	4.71	2.24
60-1.33D-33-9.89	0.021	4.88	2.42
60-1.33D-33-9.56	0.020	4.88	2.15
60-1.33D-33-9.29	0.019	4.99	2.25
60-1.33D-33-8.77	0.018	5.10	2.17
60-1.33D-66-12.22	0.026	5.61	2.98
60-1.33D-66-11.78	0.025	5.53	3.00
60-1.33D-66-11.37	0.024	5.53	2.79
60-1.33D-66-11.04	0.023	5.57	2.93
60-1.33D-66-10.69	0.022	5.60	2.98
60-1.33D-66-10.47	0.022	5.43	2.63
60-1.33D-66-10.18	0.021	5.47	2.65
60-1.33D-66-9.52	0.020	5.19	2.37
60-1.33D-99-12.12	0.025	6.09	2.84
60-1.33D-99-11.73	0.025	6.14	2.87
60-1.33D-99-10.93	0.023	6.02	2.94
60-1.33D-99-10.43	0.022	5.92	2.95
60-1.33D-99-10.16	0.021	5.91	2.96
60-1.33D-99-9.52	0.020	5.68	2.94
60-1.33D-99-9.37	0.020	5.69	2.99
60-1.33D-99-8.79	0.018	5.37	2.89
60-1.33D-99-7.82	0.016	4.95	2.72
60-1.33-33-12.25	0.026	3.30	2.46
60-1.33-33-11.76	0.025	3.16	2.48
60-1.33-33-11.02	0.023	3.45	2.43
60-1.33-33-10.5	0.022	3.60	2.48
60-1.33-33-10.2	0.021	3.56	2.33
60-1.33-33-9.48	0.020	3.59	2.30
60-1.33-33-9.23	0.019	3.57	2.35
60-1.33-33-8.7	0.018	3.64	2.24
60-1.33-33-7.77	0.016	3.69	2.14
40-1.33-33-12.25	0.026	5.21	2.33
40-1.33-33-11.68	0.024	5.37	2.26
40-1.33-33-11.25	0.024	5.36	2.32
40-1.33-33-11.02	0.023	5.33	2.17
40-1.33-33-10.54	0.022	5.06	2.23
40-1.33-33-10.08	0.021	5.22	2.13
40-1.33-33-9.77	0.020	5.02	2.19
50-1.33D-33-12.33	0.026	6.28	1.99

Table B.1 Experimental Data continued

Reference	*Q (m^3/s)*	*y_C (cm)*	*y_A (cm)*
50-1.33D-33-11.79	0.025	6.24	2.07
50-1.33D-33-11.44	0.024	6.31	2.02
50-1.33D-33-11.21	0.023	6.21	1.97
50-1.33D-99-12.12	0.025	6.58	2.64
50-1.33D-99-11.66	0.024	6.15	2.84
50-1.33D-99-11.28	0.024	5.97	2.53
50-1.33D-99-10.89	0.023	5.81	2.54
50-1.33D-99-10.5	0.022	5.58	2.58
50-1.33D-99-10.18	0.021	5.36	2.54
50-1.33D-99-9.89	0.021	5.30	2.66
50-1.33D-99-9.52	0.020	5.16	2.69
50-1.33D-99-9.1	0.019	4.79	2.61
50-1.33D-99-8.79	0.018	4.88	2.62
50-1.33D-66-12.19	0.025	6.38	3.12
50-1.33D-66-11.83	0.025	6.61	3.10
50-1.33D-66-11.42	0.024	6.31	2.89
60-2-66-14.63	0.017	2.84	1.59
60-2-66-14.12	0.016	2.83	1.61
60-2-66-13.35	0.015	2.82	1.55
60-2-66-12.04	0.014	2.82	1.59
60-2-66-10.84	0.012	2.82	1.56
60-2-66-9.88	0.011	2.84	1.56
60-2-99-16.95	0.019	2.69	2.02
60-2-99-15.98	0.018	2.70	2.00
60-2-99-15.3	0.017	2.76	1.88
60-2-99-13.98	0.016	2.76	1.75
60-2-99-13.25	0.015	2.72	1.80
60-2-99-12.04	0.014	2.72	1.85
60-2-99-11.09	0.013	2.69	1.71
60-2-99-10.34	0.012	2.69	1.63
60-2-99-8.42	0.010	2.72	1.59
40-2-66-16.39	0.019	3.47	1.86
40-2-66-15.73	0.018	3.64	1.80
40-2-66-15.47	0.018	3.75	1.77
40-2-66-14.9	0.017	3.67	1.65
40-2-66-13.84	0.016	3.79	1.68
40-2-66-13.05	0.015	3.65	1.54
40-2-66-11.7	0.013	3.56	1.43
40-2-99-17.22	0.020	4.00	2.41
40-2-99-16.15	0.018	4.03	2.60
40-2-99-14.4	0.016	4.00	2.39
40-2-99-14.03	0.016	3.83	2.43
40-2-99-12.84	0.015	3.58	2.13
40-2-99-12.26	0.014	3.55	2.06
40-2-99-11.82	0.013	3.32	1.85
50-2D-66-18.13	0.021	4.20	2.08
50-2D-66-17.14	0.020	3.99	1.80
50-2D-66-16.51	0.019	4.32	2.02
50-2D-66-15.69	0.018	4.13	1.70

Table B.1 Experimental Data continued

Reference	*Q (m^3/s)*	*y_C (cm)*	*y_A (cm)*
50-2D-66-15.26	0.017	3.97	1.65
50-2D-66-14.5	0.016	4.15	1.57
50-2D-66-13.5	0.015	4.37	1.51
50-2D-99-17.26	0.020	4.64	2.41
50-2D-99-16.71	0.019	4.59	2.35
50-2D-99-15.98	0.018	4.74	2.45
50-2D-99-15.47	0.018	4.73	2.28
50-2D-99-14.99	0.017	4.56	2.45
50-2D-99-14.4	0.016	4.77	2.34
50-2D-99-12.84	0.015	4.79	1.98
50-2-66-17.03	0.019	2.97	1.64
50-2-66-15.81	0.018	2.92	1.52
50-2-66-14.72	0.017	2.91	1.52
50-2-66-13.69	0.016	3.26	1.43
50-2-66-12.84	0.015	3.43	1.49
50-2-66-11.93	0.014	3.38	1.52
50-2-66-10.47	0.012	3.49	1.40
50-2-99-17.26	0.020	2.92	2.37
50-2-99-16.31	0.019	3.34	2.55
50-2-99-15.77	0.018	3.42	2.50
50-2-99-15.26	0.017	3.38	2.47
50-2-99-13.98	0.016	3.79	2.30
50-2-99-13	0.015	3.74	1.99
50-2-99-12.04	0.014	3.79	1.88
50-2-99-11.42	0.013	3.69	1.72
50-2-99-9.81	0.011	3.24	1.60
60-2D-99-16.71	0.019	3.77	2.35
60-2D-99-15.81	0.018	3.85	2.52
60-2D-99-15.26	0.017	3.80	2.57
60-2D-99-14.59	0.017	3.87	2.35
60-2D-99-12.79	0.015	3.98	2.01
60-2D-99-11.93	0.014	3.95	1.72
60-2D-99-10.72	0.012	4.07	1.65
60-2D-99-9.39	0.011	3.34	1.59
60-2D-66-17.79	0.020	3.69	2.02
60-2D-66-15.98	0.018	3.61	1.91
60-2D-66-14.9	0.017	3.48	1.63
60-2D-66-14.17	0.016	3.34	1.52
60-2D-66-13.55	0.015	3.49	1.46
60-2D-66-12.69	0.014	3.83	1.49
60-2D-66-11.65	0.013	3.92	1.48
60-2D-66-9.94	0.011	3.94	1.47
40-2D-66-17.87	0.020	5.87	1.28
40-2D-66-17.38	0.020	5.82	1.43
40-2D-66-17.03	0.019	5.55	1.45
40-2D-66-15.43	0.018	5.05	1.40
40-2D-66-14.12	0.016	4.66	1.35
40-2D-66-12.74	0.014	4.26	1.37
40-2D-66-11.87	0.014	3.73	1.33

Table B.1 Experimental Data continued

Reference	*Q (m^3/s)*	*y_C (cm)*	*y_A (cm)*
40-2D-99-17.9	0.020	5.87	2.47
40-2D-99-16.27	0.019	5.56	2.34
40-2D-99-15.43	0.018	4.93	2.74
40-2D-99-14.9	0.017	4.80	2.27
40-2D-99-13.98	0.016	4.29	2.28
40-1-66-9.43	0.030	6.70	2.87
40-1-66-9.04	0.029	6.84	2.90
40-1-66-8.72	0.028	6.50	2.88
40-1-66-8.18	0.026	6.37	2.79
40-1-66-7.77	0.025	6.19	2.89
40-1-66-7.46	0.024	6.02	2.87
40-1-33-9.39	0.030	6.75	2.57
40-1-33-8.83	0.028	7.08	2.65
40-1-33-8.79	0.028	6.66	2.51
40-1-33-8.18	0.026	6.70	2.50
40-1-33-8.01	0.026	6.56	2.58
40-1-33-7.67	0.025	6.33	2.58
40-1-33-7.49	0.024	6.20	2.50
60-1-66-9.31	0.030	5.42	3.34
60-1-66-8.87	0.029	5.45	3.39
60-1-66-8.78	0.028	5.48	3.28
60-1-66-8.4	0.027	5.41	3.23
60-1-66-8	0.026	5.45	3.19
60-1-66-7.6	0.024	5.49	3.14
60-1-66-7.07	0.023	5.55	3.11
60-1-66-6.57	0.021	5.23	3.04
60-1-66-5.87	0.019	4.96	3.22
60-1-33-9.3	0.030	5.20	2.66
60-1-33-8.9	0.029	5.26	2.58
60-1-33-8.47	0.027	5.11	2.80
60-1-33-8.3	0.027	5.25	2.65
60-1-33-7.75	0.025	5.17	2.79
60-1-33-7.18	0.023	5.20	2.82
60-1-33-6.8	0.022	5.16	2.73
60-1-33-6.16	0.020	5.20	2.75
50-1-66-9.31	0.030	6.66	3.10
50-1-66-8.84	0.028	6.64	3.32
50-1-66-8.36	0.027	6.43	3.24
50-1-66-7.9	0.025	6.27	3.31
50-1-66-7.42	0.024	6.26	3.23
50-1-66-6.9	0.022	5.74	2.96
50-1-66-6.3	0.020	5.26	3.02
50-1-33-9.35	0.030	6.21	2.63
50-1-33-8.95	0.029	5.99	2.73
50-1-33-8.77	0.028	6.02	2.57
50-1-33-8.58	0.028	5.99	2.53
50-1-33-8.18	0.026	5.88	2.51
50-1-33-7.75	0.025	5.96	2.50
50-1-33-7.45	0.024	5.84	2.49

Table B.1 Experimental Data continued

Reference	***Q (m^3/s)***	***y_C (cm)***	***y_A (cm)***
50-1D-33-9.3	0.030	7.95	2.59
50-1D-33-8.88	0.029	7.88	2.69
50-1D-33-8.52	0.027	7.73	2.61
50-1D-33-8.23	0.026	7.82	2.49
50-1D-33-7.96	0.026	7.20	2.60
50-1D-33-7.67	0.025	7.11	2.56
50-1D-33-7.14	0.023	6.59	2.49
50-1D-33-6.56	0.021	6.11	2.45
50-1D-66-9.11	0.029	7.50	2.77
50-1D-66-8.75	0.028	7.20	2.97
50-1D-66-8.42	0.027	6.95	2.86
50-1D-66-8.07	0.026	6.81	2.92
50-1D-66-7.85	0.025	6.32	2.88
50-1D-66-7.69	0.025	6.32	2.96
50-1D-66-7.18	0.023	6.01	2.86
60-1D-33-9.29	0.030	6.97	2.67
60-1D-33-8.78	0.028	7.00	2.55
60-1D-33-8.08	0.026	6.75	2.52
60-1D-33-8.07	0.026	6.26	2.39
60-1D-33-7.34	0.024	6.69	2.47
60-1D-33-6.74	0.022	6.37	2.51
60-1D-33-6.29	0.020	6.22	2.46
60-1D-33-5.82	0.019	5.58	2.58
60-1D-66-9.42	0.030	7.43	3.02
60-1D-66-8.96	0.029	7.30	3.28
60-1D-66-8.75	0.028	7.29	3.25
60-1D-66-8.24	0.027	7.12	3.29
60-1D-66-7.7	0.025	7.03	3.52
60-1D-66-7.27	0.023	6.54	3.14
60-1D-66-6.65	0.021	6.16	3.01
40-1D-66-10.28	0.033	6.84	2.78